MIKE 21 Flow Model FM

Hydrodynamic and Transport module

Scientific Documentation

DHI A/S headquarters
Agern Allé 5
DK-2970 Hørsholm
Denmark

+45 4516 9200 Telephone
mike@dhigroup.com
www.mikepoweredbydhi.com

Company Registration No.: DK36466871

PLEASE NOTE

COPYRIGHT

LIMITED LIABILITY

The liability of DHI is limited as specified in your DHI Software License Agreement:

In no event shall DHI or its representatives (agents and suppliers) be liable for any damages whatsoever including, without limitation, special, indirect, incidental or consequential damages or damages for loss of business profits or savings, business interruption, loss of business information or other pecuniary loss arising in connection with the Agreement, e.g. out of Licensee's use of or the inability to use the Software, even if DHI has been advised of the possibility of such damages.

This limitation shall apply to claims of personal injury to the extent permitted by law. Some jurisdictions do not allow the exclusion or limitation of liability for consequential, special, indirect, incidental damages and, accordingly, some portions of these limitations may not apply.

Notwithstanding the above, DHI's total liability (whether in contract, tort, including negligence, or otherwise) under or in connection with the Agreement shall in aggregate during the term not exceed the lesser of EUR 10.000 or the fees paid by Licensee under the Agreement during the 12 months' period previous to the event giving rise to a claim.

Licensee acknowledge that the liability limitations and exclusions set out in the Agreement reflect the allocation of risk negotiated and agreed by the parties and that DHI would not enter into the Agreement without these limitations and exclusions on its liability. These limitations and exclusions will apply notwithstanding any failure of essential purpose of any limited remedy.

CONTENTS

MIKE 21 Flow Model FM
Hydrodynamic and Transport Module
Scientific Documentation

APPENDICES

1 Introduction

This document presents the scientific background for the MIKE 21 Flow Model FM. The objective is to provide the user with a detailed description of the governing equations, numerical discretization and solution methods.

MIKE 21 Flow Model FM has been developed for applications within oceanographic, coastal and estuarine environments.

The model is based on the numerical solution of the two-dimensional shallow water equations. Thus, the model consists of continuity and momentum equations. The spatial discretization of the governing equations in conserved form is performed using a cell-centered finite volume method. The time integration is performed using an explicit scheme. Here either a first-order Euler method or a second-order explicit Runge-Kutta scheme can be applied. The interface convective fluxes are calculated using an approximate Riemann solver. This shock-capturing scheme enables robust and stable simulation of flows involving shocks or discontinuities such as bores and hydraulic jumps.

2 Governing equations

The governing equations are solved in a Cartesian coordinate system. The governing equations can also be formulated in a spherical coordinate system. For more details, see Appendix A. The governing equations for porous media are presented in Appendix B.

2.1 Governing equations in a Cartesian coordinate system

2.1.1 Shallow water equations

The two-dimensional shallow water equations are obtained by assuming a hydrostatic pressure distribution and integrating the Navier–Stokes equations over the water depth. A description of the Navier-Stokes equations can be found in the scientific documentation for MIKE 3 Flow Model FM. For more detail on the derivation of the two-dimensional shallow water equations see Vreugdenhill (1994). The two-dimensional shallow water equations in conservative form can expressed as

$$\frac{\partial h}{\partial t}+\frac{\partial hu}{\partial x}+\frac{\partial hv}{\partial y}=0 \tag{2.1}$$

$$\frac{\partial hu}{\partial t}+\frac{\partial hu^2}{\partial x}+\frac{\partial huv}{\partial y}= fhv-gh\frac{\partial \eta}{\partial x}-\frac{h}{\rho_0}\frac{\partial p_A}{\partial \mathrm{x}}-\frac{gh^2}{2\rho_0}\frac{\partial \rho}{\partial x}-\frac{\tau_{fx}}{\rho_0}+\frac{\tau_{sx}}{\rho_0}-F_{vx}+\frac{\partial hT_{xx}}{\partial x}+\frac{\partial hT_{xy}}{\partial y} \tag{2.2}$$

$$\frac{\partial hv}{\partial t}+\frac{\partial hvu}{\partial x}+\frac{\partial hv^2}{\partial y}= -fhu-gh\frac{\partial \eta}{\partial y}-\frac{h}{\rho_0}\frac{\partial p_A}{\partial y}-\frac{gh^2}{2\rho_0}\frac{\partial \rho}{\partial y}-\frac{\tau_{fy}}{\rho_0}+\frac{\tau_{sy}}{\rho_0}-F_{vy}+\frac{\partial hT_{xy}}{\partial x}+\frac{\partial hT_{yy}}{\partial y} \tag{2.3}$$

Here t is the time; x and y are the Cartesian coordinates; $h=\eta+d$ is the total water depth, where η is the surface elevation and d is the still water depth; u and v are the depth averaged velocity components in the x and y direction; $f=2\Omega sin\phi$ is the Coriolis parameter (Ω is the angular rate of revolution and ϕ the geographic latitude); g is the gravitational acceleration; p_A is the atmospheric pressure at the free surface; ρ is the density of water; ρ_0 is the reference density of water. (τ_{fx},τ_{fy}) are the x- and y-components of the stresses due to bottom friction, surface friction and flow resistance (see section 4.1, 4.3, 4.6). and (τ_{sx},τ_{sy}) are the x- and y-components of the surface stresses due to the wind (see section 4.5). $\boldsymbol{F}_v=(F_{vx},F_{vy})$ is the drag force due to vegetation (see section 4.4). The lateral stresses, T_{xx}, T_{xy} and T_{yy}, include viscous friction, turbulent friction and differential advection. They are estimated using an eddy viscosity formulation based on the depth averaged velocities

$$T_{xx}=2\nu\frac{\partial u}{\partial x} \qquad T_{xy}=\nu\left(\frac{\partial u}{\partial y}+\frac{\partial v}{\partial x}\right) \qquad T_{yy}=2\nu\frac{\partial u}{\partial y} \tag{2.4}$$

where ν is the eddy viscosity. The fluid is assumed to be incompressible. Hence, the density does not depend on the pressure, but only on the temperature, T and the salinity, S, via the equation of state

$$\rho=\rho(S,T) \tag{2.5}$$

Here the UNESCO equation of state is used (see UNESCO,1981).

To give a conservative formulation, the gravity surface terms are split into two terms (see Chippada (1998), Rogers (2001), Quecedo (2002), Liang or Borthwick (2009))

$$gh\frac{\partial \eta}{\partial x} = \frac{1}{2}g\frac{\partial (h^2 - d^2)}{\partial x} - g\eta\frac{\partial d}{\partial x} = \frac{1}{2}g\frac{\partial (\eta^2 + 2\eta d)}{\partial x} - g\eta\frac{\partial d}{\partial x} \tag{2.6}$$

$$gh\frac{\partial \eta}{\partial y} = \frac{1}{2}g\frac{\partial (h^2 - d^2)}{\partial y} - g\eta\frac{\partial d}{\partial y} = \frac{1}{2}g\frac{\partial (\eta^2 + 2\eta d)}{\partial y} - g\eta\frac{\partial d}{\partial y} \tag{2.7}$$

It is easily seen that if η is constant, the two terms cancel exactly. In the discrete case, this is also true if the two derivatives are calculated using the same scheme.

In matrix form the continuity equation and the momentum equations may be written

$$\frac{\partial \boldsymbol{U}}{\partial t} + \nabla \cdot \boldsymbol{F} = \boldsymbol{S_0} + \boldsymbol{S_f} \tag{2.8}$$

Here $\boldsymbol{U} = (h, hu, hv)^T$ and $\boldsymbol{F} = \boldsymbol{F}^c - \boldsymbol{F}^d = (\boldsymbol{F}^x, \boldsymbol{F}^y)^T$. The flux components and the source terms can be written

$$\boldsymbol{F}_x^c = \begin{pmatrix} hu \\ huu + \frac{1}{2}g(\eta^2 + 2\eta d) \\ hvu \end{pmatrix} \quad \boldsymbol{F}_y^c = \begin{pmatrix} hv \\ huv \\ hvv + \frac{1}{2}g(\eta^2 + 2\eta d) \end{pmatrix} \tag{2.9}$$

$$\boldsymbol{F}_x^d = \begin{pmatrix} 0 \\ 2hv\frac{\partial u}{\partial x} \\ hv\left(\frac{\partial u}{\partial y} + \frac{\partial v}{\partial x}\right) \end{pmatrix} \quad \boldsymbol{F}_y^d = \begin{pmatrix} 0 \\ hv\left(\frac{\partial u}{\partial y} + \frac{\partial v}{\partial x}\right) \\ 2hv\frac{\partial v}{\partial y} \end{pmatrix} \tag{2.10}$$

$$\boldsymbol{S_0} = \begin{pmatrix} 0 \\ g\eta\frac{\partial d}{\partial x} + fhv - \frac{h}{\rho_0}\frac{\partial p_A}{\partial x} - \frac{gh^2}{2\rho_0}\frac{\partial \rho}{\partial x} + \frac{\tau_{sx}}{\rho_0} \\ g\eta\frac{\partial d}{\partial y} - fhu - \frac{h}{\rho_0}\frac{\partial p_A}{\partial y} - \frac{gh^2}{2\rho_0}\frac{\partial \rho}{\partial y} + \frac{\tau_{sy}}{\rho_0} \end{pmatrix} \quad \boldsymbol{S_f} = \begin{pmatrix} 0 \\ -\frac{\tau_{fx}}{\rho_0} - F_{vx} \\ -\frac{\tau_{fy}}{\rho_0} - F_{vy} \end{pmatrix} \tag{2.11}$$

2.1.2 Transport equations for temperature and salinity

The transport of temperature and salinity follows the general advection-diffusion equation as

$$\frac{\partial hT}{\partial t} + \frac{\partial huT}{\partial x} + \frac{\partial hvT}{\partial y} = \frac{\partial}{\partial x}\left(hD_{ts}\frac{\partial T}{\partial x}\right) + \frac{\partial}{\partial y}\left(hD_{ts}\frac{\partial T}{\partial y}\right) + h\widehat{H} \tag{2.12}$$

$$\frac{\partial hS}{\partial t} + \frac{\partial huS}{\partial x} + \frac{\partial hvS}{\partial y} = \frac{\partial}{\partial x}\left(hD_{ts}\frac{\partial S}{\partial x}\right) + \frac{\partial}{\partial y}\left(hD_{ts}\frac{\partial S}{\partial y}\right) \tag{2.13}$$

where T is the depth averaged temperature, S is the depth averaged salinity and $\widehat{H}$ is a source term due to heat exchange with the atmosphere (see section 4.12). D_{ts} is the diffusion coefficient. The diffusion coefficient can be a constant value or determined as the scaled eddy viscosity.

In matrix form the transport equations for T and s may be written

$$\frac{\partial \boldsymbol{U}}{\partial t} + \nabla \cdot \boldsymbol{F} = \boldsymbol{S} \tag{2.14}$$

where $\boldsymbol{U} = (hT,\ hS)^T$ and $\boldsymbol{F} = \boldsymbol{F^c} - \boldsymbol{F^d} = (\boldsymbol{F}_x, \boldsymbol{F}_y)^T$. The flux components and the source terms can be written

$$\boldsymbol{F}_x^c = \begin{pmatrix} huT \\ huS \end{pmatrix} \quad \boldsymbol{F}_y^c = \begin{pmatrix} hvT \\ hvS \end{pmatrix} \tag{2.15}$$

$$\boldsymbol{F}_x^d = \begin{pmatrix} hD_{ts}\dfrac{\partial T}{\partial x} \\ hD_{ts}\dfrac{\partial S}{\partial x} \end{pmatrix} \quad \boldsymbol{F}_y^d = \begin{pmatrix} hD_{ts}\dfrac{\partial T}{\partial y} \\ hD_{ts}\dfrac{\partial S}{\partial y} \end{pmatrix} \tag{2.16}$$

$$\boldsymbol{S} = \begin{pmatrix} h\hat{H} \\ 0 \end{pmatrix} \tag{2.17}$$

2.1.3 Transport equation for a scalar quantity

The conservation equation for a scalar quantity is given by

$$\frac{\partial hC}{\partial t} + \frac{\partial huC}{\partial x} + \frac{\partial hvC}{\partial y} = \frac{\partial}{\partial x}\left(hD_c\frac{\partial C}{\partial x}\right) + \frac{\partial}{\partial y}\left(hD_c\frac{\partial C}{\partial y}\right) - hk_pC \tag{2.18}$$

where C is the depth averaged concentration of the scalar quantity and k_p is the linear decay rate of the scalar quantity. D_c is the diffusion coefficient. The diffusion coefficient can be a constant value or determined as the scaled eddy viscosity.

In matrix form the transport equations for C may be written

$$\frac{\partial \boldsymbol{U}}{\partial t} + \nabla \cdot \boldsymbol{F} = \boldsymbol{S} \tag{2.19}$$

Where $\boldsymbol{U} = (hC)$ and $\boldsymbol{F} = \boldsymbol{F^c} - \boldsymbol{F^d} = (\boldsymbol{F}_x, \boldsymbol{F}_y)^T$. The flux components and the source terms can be written

$$\boldsymbol{F}_x^c = (huC) \quad \boldsymbol{F}_y^c = (hvC) \tag{2.20}$$

$$\boldsymbol{F}_x^d = \left(hD_c\frac{\partial C}{\partial x}\right) \quad \boldsymbol{F}_y^d = \left(hD_c\frac{\partial C}{\partial y}\right) \tag{2.21}$$

$$\mathrm{S} = -\left(hk_pC\right) \tag{2.22}$$

3 Numerical method

The discretization in solution domain is performed using a cell-centered finite volume method (CCFV). The spatial domain is discretized by subdivision of the continuum into non-overlapping control volumes and by evaluating the field equations in integral form on these cells.

3.1 Mesh and discretization scheme

3.1.1 Mesh

The computational mesh is based on the unstructured meshes approach, which gives the maximum degree of flexibility. Control of node distribution allows for optimal usage of nodes and adaptation of mesh resolution to the relevant physical scales. The use of unstructured meshes also makes it possible to handle problems characterized by computational domains with complex boundaries.

The elements in the mesh can be triangles, quadrilateral elements or a combination of these (see Figure 3.1).

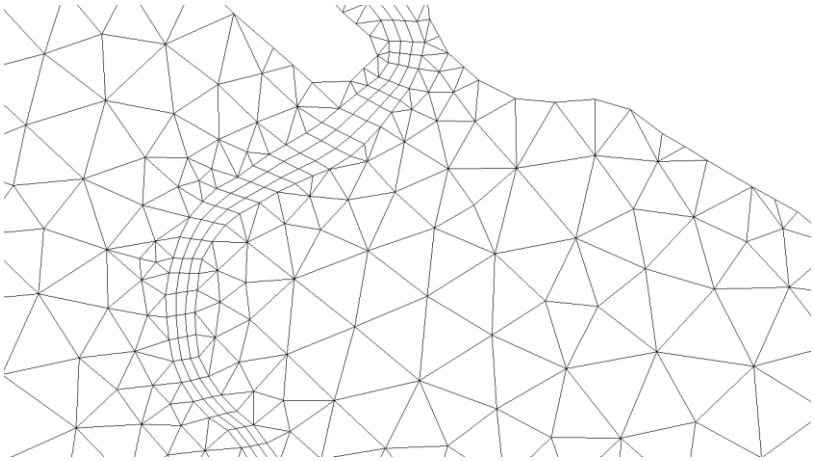

Figure 3.1 Unstructured mesh with both triangular and quadrilateral elements.

3.1.2 Discretization scheme

The discrete solution for the water depth, h, for the velocity components, u and v, and the transport variables, T, S and C, are defined at the centroid of the elements in the mesh.

3.2 Finite volume method

The matrix form of the governing equations presented in Chapter 2 can be written as

$$\frac{\partial \boldsymbol{U}}{\partial t} + \nabla \cdot \boldsymbol{F}(\boldsymbol{U}) = \boldsymbol{S} \tag{3.1}$$

Integrating Eq. 3. 1 over the *i*th cell and using Gauss's theorem to rewrite the flux integral gives

$$\int_{A_i} \frac{\partial \boldsymbol{U}}{\partial t} d\Omega + \int_{\Gamma_i} (\boldsymbol{F}(\boldsymbol{U}) \cdot \boldsymbol{n})\, ds = \int_{A_i} \boldsymbol{S}(\boldsymbol{U}) d\Omega \tag{3.2}$$

where A is the area of the *i*th cell, Ω is the integration variable defined on A_i, Γ_i is the boundary of the *i*th cell and s is the integration variable along the boundary. $\boldsymbol{n} = (n_x, n_y)^T$ is the unit outward normal vector along the boundary. Evaluating the area integrals by a one-point quadrature rule, the quadrature point being the centroid of the cell, and evaluating the boundary integral using a mid-point quadrature rule, Eq. 3.2 can be written

$$\frac{\partial \boldsymbol{U}_i}{\partial t} + \frac{1}{A_i} \sum_{j}^{NF} \boldsymbol{F} \cdot \boldsymbol{n}_{ij} \Delta s_{ij} = \boldsymbol{S}_i \tag{3.3}$$

Here $\boldsymbol{U}_i$ and $\boldsymbol{S}_i$, respectively, are average values of $\boldsymbol{U}$ and $\boldsymbol{S}$ over the *i*th cell and stored at the cell centre. NF is the number of faces of the cell and the face ij is common to the cells associated with $\boldsymbol{U}_i$ and $\boldsymbol{U}_j$. Δs_{ij} is the length of the face ij, and $\boldsymbol{n}_{ij}$ is the restriction of $\boldsymbol{n}$ to the face ij.

3.3 Numerical solution of the flow equations

3.3.1 Space discretization of the shallow water equations

The space discretization is performed using the finite volume method as described in Section 3.2. The normal convective flux $\boldsymbol{F}_n(\boldsymbol{U}_L, \boldsymbol{U}_R) = \boldsymbol{F}(\boldsymbol{U}_L, \boldsymbol{U}_R) \cdot \boldsymbol{n_{ij}}$ across a face ij is determined using an approximate Riemann solver. The Riemann solver uses the variable $\boldsymbol{U} = (h, hu, hv)^T$ to the left and right of the face. The diffusive flux at the cell interfaces is approximated by a central scheme.

Reconstruction of face values

The variables, $\boldsymbol{U}_L$ and $\boldsymbol{U}_R$, to the left and right of a face are reconstructed from the cell values, $\boldsymbol{U}_i$ and $\boldsymbol{U}_j$, in two steps.

In the first step, the variables $\boldsymbol{U}_l$ and $\boldsymbol{U}_r$ are determined from element values. For a first order scheme, $\boldsymbol{U}_l = \boldsymbol{U}_i$ and $\boldsymbol{U}_r = \boldsymbol{U}_j$. Second-order spatial accuracy is achieved by employing a linear gradient-reconstruction technique for the primitive variables η, u and v. The face value at the vertical faces for a variable q in cell i is obtained by

$$q_l = q_i + \nabla q_i \cdot \boldsymbol{r}_{if}\,, \qquad q_r = q_j + \nabla q_j \cdot \boldsymbol{r}_{jf} \tag{3.4}$$

where $\boldsymbol{r}_{if}$ is the distance vector from the cell centre to the face and ∇q_i is the gradient vector. For estimation of the gradient vector, the Green-Gauss gradient approach is utilized. Here, the procedure proposed by Jawahar and Kamath (2000) is used. This procedure is based on a wide computational stencil to improve accuracy also for meshes with poor connectivity. The vertex (node) value is computed using the pseudo-Laplacian procedure proposed by Holmes and Connell (1989). To avoid numerical oscillations a second order TVD slope limiter (Van Leer limiter, see Hirch, 1990 and Darwish, 2003) is used.

For a second-order scheme, the water depth d is also reconstructed at each side of the face using eq. (3.4) and then the total water depths at the left and right of the face are defined as

$$h_l = \max(0, \eta_l + d_l), \qquad h_r = \max(0, \eta_r + d_r) \tag{3.5}$$

In the second step, the variables $\boldsymbol{U}_L$ and $\boldsymbol{U}_R$ are determined from $\boldsymbol{U}_l$ and $\boldsymbol{U}_r$. The water depth is assigned the same value at both sides of the face, $d_f = d_L = d_R$. Depending on the total water depth, two different techniques are used. As default, the average value of water depth is used

$$d_f = \frac{1}{2}(d_l + d_r) \tag{3.6}$$

and the total water depths are defined by

$$h_L = \max(\eta_l + d_f, 0), \qquad h_R = \max(\eta_r + d_f, 0). \tag{3.7}$$

If the total water height on either side is smaller than the difference in water depth, that is, if $h_l < |d_r - d_l|$ or $h_r < |d_r - d_l|$, the water depth is instead defined as in Chen & Noelle (2017) by

$$d_f = -\min(-\min(d_l, d_r), \min(\eta_l, \eta_r)) \tag{3.8}$$

and the total water depths are defined by

$$h_L = \min(\eta_l + d_f, h_l), \qquad h_R = \min(\eta_r + d_f, h_r). \tag{3.9}$$

Finally, the fluxes at each side of the face are determined from the velocities u_l, v_l, u_r, v_r and the total water depths h_L, h_R.

Riemann solver

The normal convective flux $\boldsymbol{F}_n(\boldsymbol{U})$ at the faces can be written

$$\boldsymbol{F}_n(\boldsymbol{U}) = \begin{pmatrix} hu_\perp \\ huu_\perp + \frac{1}{2}g(\eta^2 + 2\eta d)n_x \\ hvu_\perp + \frac{1}{2}g(\eta^2 + 2\eta d)n_y \end{pmatrix} \tag{3.10}$$

where $\boldsymbol{U} = (h, hu, hv)^T$ is the solution vector, and $u_\perp = un_x + vn_y$ is the velocity perpendicular to the cell face. This flux is reconstructed at cell-interfaces using the HLLC scheme introduced by Toro et al. (1994) for solving the Euler equations. The shock-capturing scheme enables robust and stable simulation of flows involving shocks or discontinuities such as bores and hydraulic jumps. The interface flux is computed as follows (see Toro (2001))

$$\boldsymbol{F}(\boldsymbol{U}_L, \boldsymbol{U}_R) \cdot \boldsymbol{n} = \begin{cases} \boldsymbol{F}_L & if\ S_L \geq 0 \\ \boldsymbol{F}_{*L} & if\ S_L < 0 \leq S_* \\ \boldsymbol{F}_{*R} & if\ S_* < 0 \leq S_R \\ \boldsymbol{F}_R & if\ S_R \leq 0 \end{cases} \tag{3.11}$$

where $\boldsymbol{F}_L = \boldsymbol{F}_n(\boldsymbol{U}_L)$ and $\boldsymbol{F}_R = \boldsymbol{F}_n(\boldsymbol{U}_R)$ are calculated from Eq. (3.10), and the middle region fluxes, $\boldsymbol{F}_{*L}$ and $\boldsymbol{F}_{*R}$ are given by

$$\boldsymbol{F}_{*L} = \begin{pmatrix} e_1 \\ e_2 n_x - u_{\parallel L} e_1 n_y \\ e_2 n_y + u_{\parallel L} e_1 n_x \end{pmatrix} \tag{3.12}$$

$$\boldsymbol{F}_{*R} = \begin{pmatrix} e_1 \\ e_2 n_x - u_{\parallel R} e_1 n_y \\ e_2 n_y + u_{\parallel R} e_1 n_x \end{pmatrix} \tag{3.13}$$

Here $u_\parallel = -un_y + vn_x$ is the velocity tangential to the cell face, and (e_1, e_2) is the component of the normal flux which is calculated using the HLL solver proposed by Harten et al. (1983)

$$\boldsymbol{E} = \frac{S_R \widehat{\boldsymbol{E}}_L - S_L \widehat{\boldsymbol{E}}_R + f_{HLLC} S_L S_R \left(\widehat{\boldsymbol{U}}_R - \widehat{\boldsymbol{U}}_L\right)}{S_R - S_L} \tag{3.14}$$

Here $\widehat{\boldsymbol{U}} = (h, hu_\perp)^T$ and $\widehat{\boldsymbol{E}} = \left(hu_\perp, hu_\perp u_\perp + \frac{1}{2} g(\eta^2 + 2\eta d)\right)^T$. To be able to scale the damping introduced by the HLLC solver a scaling factor f_{HLLC} has been introduced, where the factor must be in the interval [0,1]. The scaling factor, $f_{HLLC} = 1$, corresponds to the standard HLLC solver.

An appropriate method for approximating the wave speeds is essential for the efficiency of the HLLC solver. Different approximations can be found in the literature, e.g. Fraccarollo and Toro (1994). Here the approach used by Song et al. (2011) is used

$$S_L = \begin{cases} u_{\perp R} - 2\sqrt{g h_R} & h_L = 0 \\ min\left(u_{\perp L} - \sqrt{g h_L}, u_{\perp *} - \sqrt{g h_*}\right) & h_L > 0 \end{cases} \tag{3.15}$$

and

$$S_R = \begin{cases} u_{\perp L} + 2\sqrt{g h_L} & h_R = 0 \\ max\left(u_{\perp R} + \sqrt{g h_R}, u_{\perp *} + \sqrt{g h_*}\right) & h_R > 0 \end{cases} \tag{3.16}$$

where the Roe-averaged quantities

$$u_{\perp *} = \frac{u_{\perp L}\sqrt{h_L} + u_{\perp R}\sqrt{h_R}}{\sqrt{h_L} + \sqrt{h_R}} \tag{3.17}$$

$$h_* = \frac{1}{2}(h_L + h_R) \tag{3.18}$$

The wave speed S_* is given by the

$$S_* = \frac{S_L h_R (u_{\perp R} - S_R) - S_R h_L (u_{\perp L} - S_L)}{h_R (u_{\perp R} - S_R) - h_L (u_{\perp L} - S_L)} \tag{3.19}$$

3.3.2 Time integration of the shallow water equations

The time integration of the shallow water equations is performed using an explicit scheme. Here either a first-order explicit Euler scheme or a two-stage explicit second-

order Runge-Kutta scheme (the midpoint method) are applied. The integration procedure for the explicit Euler scheme is

$$\frac{\boldsymbol{U}^{n+1}-\boldsymbol{U}^{n}}{\Delta t}=-\left(\frac{\partial \boldsymbol{F}_x}{\partial x'}+\frac{\partial \boldsymbol{F}_y}{\partial y'}\right)^{n}+\boldsymbol{S}_0^{n}+\boldsymbol{S}_f^{n+1} \tag{3.20}$$

The special treatment of the friction source term is discussed in section 3.3.3. The integration procedure for the two-stage explicit Runge-Kutta scheme is

Stage 1:

$$\frac{\boldsymbol{U}^{n+1/2}-\boldsymbol{U}^{n}}{\Delta t/2}=-\left(\frac{\partial \boldsymbol{F}_x}{\partial x}+\frac{\partial \boldsymbol{F}_y}{\partial y}\right)^{n}+\boldsymbol{S}_0^{n}+\boldsymbol{S}_f^{n+1/2} \tag{3.21}$$

Stage 2:

$$\frac{\boldsymbol{U}^{n+1}-\boldsymbol{U}^{n}}{\Delta t}=-\left(\frac{\partial \boldsymbol{F}_x}{\partial x}+\frac{\partial \boldsymbol{F}_y}{\partial y}\right)^{n+1/2}+\boldsymbol{S}_0^{n+1/2}+\boldsymbol{S}_f^{n+1} \tag{3.22}$$

Due to the explicit scheme, the time step interval, Δt, is restricted by the Courant-Friedrichs-Lewy (CFL) condition

$$C=\Delta t\frac{\left(\sqrt{gh}+|u|\right)+\left(\sqrt{gh}+|v|\right)}{\Delta l}\leq C_{max} \tag{3.23}$$

where C is the Courant number and Δl is a characteristic length. C_{max} is the maximum Courant number and must be less than or equal to 1. A variable time step interval is used in the time integration of the shallow water equations and determined so that the Courant number is less than a maximum Courant number in all computational nodes. The characteristic length for a quadrilateral element, is determined as the area of the element divided by the longest edge length of the element. For a triangular element, the characteristic length is two times the area divided by the longest edge length.

3.3.3 Friction source term discretization

The contribution to the source term due to bed resistance, surface resistance (ice) and flow resistance can be written (see section 4.1, 4.3, 4.6)

$$\boldsymbol{S}_f=\begin{pmatrix} c_{fb}|\boldsymbol{u}|u+c_{fs}|\boldsymbol{u}|u+\frac{\tau_0}{\rho_0}\frac{u}{|\boldsymbol{u}|} \\ c_{fb}|\boldsymbol{u}|v+c_{fs}|\boldsymbol{u}|v+\frac{\tau_0}{\rho_0}\frac{v}{|\boldsymbol{u}|} \end{pmatrix} \tag{3.24}$$

A fully explicit treatment of the friction terms can cause instability for very shallow water. Hence, this term is treated fully implicit. For each element at each stage in the time integration procedure the water depth is updated and then the two momentum equations are solved using a Newton-Raphson method. The stopping criteria is that the 2-norm of the residual vector is less than 10^{-10}.

3.3.4 Explicit filtering

The collocated grid discretization in combination with unstructured triangular meshes is known to produce checkerboard oscillations in the horizontal velocity field, when the

higher-order scheme is applied in space. A number of methods has been proposed to solve this problem (see Wolfram and Fringer (2013), Zhang et al. (2014). Here, a filtering procedure is applied.

An explicit filtering of the horizontal velocity field is performed using the following simple approach

$$u_i = (1-f)u_i + f\bar{u}_i$$
$$v_i = (1-f)v_i + f\bar{v}_i \quad (3.25)$$

where (u_i, v_i) is the horizontal velocity components in element i, $(\bar{u}_i, \bar{v}_i)$ is the mean velocity components calculated as an area-weighted mean value of the discrete velocity components in element i and the neighboring elements. f is a filter factor. A typical value of the filter factor is in the range from 0.001 to 0.02. The filtering is performed at each stage in the time integration.

3.3.5 Flooding and drying

The approach for treatment of the moving boundaries (flooding and drying fronts) problem is based on the work by Zhao et al. (1994) and Sleigh et al. (1998). When the depths are small the problem is reformulated, and only when the depths are very small the elements/cells are removed from the calculation. The reformulation is made by setting the momentum fluxes to zero and only taking the mass fluxes into consideration.

The depth in each element is monitored and the elements are classified as dry, partially dry or wet. Also, the element faces are monitored to identify flooded element faces.

- An element face is defined as flooded if the water depth at one side of a face is less than a tolerance depth, h_{dry}, and the water depth at the other side of the face is larger than a tolerance depth, h_{wet}.
- An element is dry if the water depth is less than a tolerance depth, h_{dry}, and none of the element faces are flooded faces. The element is removed from the calculation.
- An element is partially dry if the water depth is larger than h_{dry} and less than a tolerance depth, h_{wet}, or when the depth is less than h_{dry}, and one of the element faces is a flooded face. The momentum fluxes are set to zero, and only the mass fluxes are calculated.
- An element is wet if the water depth is bigger than h_{wet}. Both the mass flux and the momentum flux are calculated.

A non-physical flow across the face will be introduced for a flooded face when the surface elevation in the wet element on one side of the face is lower than the bed level in the partially wet element on the other side. To overcome this problem the face will be treated as a closed boundary (Section 3.3.6).

In case the water depth becomes negative, the water depth is set to zero, and the water is subtracted from the adjacent elements to maintain mass balance. When this occur the water depth at the adjacent elements may become negative. Therefore, an iterative correction of the water depth is applied (max. 100 iterations). Normally only one or a few correction steps are needed.

3.3.6 Boundary conditions

At the lateral closed (solid) boundaries a free-slip boundary condition is imposed for the velocities: The normal flux is zero, and the tangential stress is set to zero. The normal flux at a closed boundary is therefore given as

$$\boldsymbol{F}_n(\boldsymbol{U}) = \begin{pmatrix} 0 \\ \frac{1}{2}g(\eta^2 + 2\eta d)n_x \\ \frac{1}{2}g(\eta^2 + 2\eta d)n_y \end{pmatrix} \tag{3.26}$$

For the flow equations a number of different boundary conditions can be applied. The level boundary condition is imposed using a strong approach based on the characteristic theory (see e.g. Sleigh et al., 1998).

The discharge boundary condition is imposed using both a strong approach based on the characteristic theory (see e.g. Sleigh et al., 1998) and a weak formulation using ghost cell technique. For the ghost cell technique, the primitive variables in the ghost cell are specified. The water level is evaluated based on the value of the adjacent interior cell, and the velocities are evaluated based on the boundary information. For a discharge boundary, the transverse velocity is set to zero for inflow and passively advected for outflow. The boundary flux is then calculated using an approximate Riemann solver. Note that using the weak formulation for a discharge boundary the effective discharge over the boundary may deviate from the specified discharge.

The free outflow boundary condition is also imposed using a weak approach. The primitive variables in the ghost cell are evaluated based on the value of the adjacent interior cell. A simple Neumann condition is applied where the gradient of the water level and velocities are zero.

The flux, velocity and Flather boundary conditions are all imposed using a weak approach. The Flather (1976) condition is one of the most efficient open boundary conditions. It is very efficient in connection with downscaling coarse model simulations to local areas (see Oddo and Pinardi (2007)). The instabilities, which are often observed when imposing stratified density at a water level boundary, can be avoided using Flather conditions

3.4 Numerical solution of the transport equations

3.4.1 Spatial discretization

Using the first-order scheme for the spatial discretization the normal flux due to the convective terms at the faces is calculated using simple upwinding. It is calculated as the mass flux times the concentration at the element in the upwind direction. The numerical damping using the first order scheme is quite high. The advantage is that there is no overshooting or undershooting, which for some applications is very important.
Using the second-order scheme for the spatial discretization a higher-order upwind scheme is applied. The concentration at the faces is determined using a linear gradient reconstruction technique based on the concentration and the gradient of the concentration at the element in the upwind direction. The gradient is determined using a wide computational stencil (see section 3.3.1). To provide stability and minimize oscillatory effects, the gradient limiter proposed by Barth and Jespersen (1989) is applied to limit the

horizontal gradients. This approach significantly reduces the numerical damping compared to the first-order scheme.

3.4.2 Time integration

The time integration is performed using either a first order explicit Euler method or a second-order explicit Runge-Kutta scheme (the midpoint method). For details of the time integration methods, see Lambert (1973) and Hirsch (1990).

Due to the explicit scheme, the time step interval, Δt, is restricted by the Courant-Friedrichs-Lewy (CFL) condition

$$C = \Delta t \frac{|u| + |v|}{\Delta l} \leq C_{max} \tag{3.27}$$

where C is the Courant number and Δl is a characteristic length. C_{max} is the maximum Courant number and must be less than or equal to 1. A variable time step interval is used in the time integration of the transport equations for temperature and salinity and the transport equation for a scalar quantity and determined so that the Courant number is less than a maximum Courant number in all computational nodes. The characteristic length for a quadrilateral element is determined as the area of the element divided by the longest edge length of the element. For a triangular element the characteristic length is two times the area divided by the longest edge length.

3.4.3 Boundary conditions

For lateral closed (solid) boundaries the normal convective flux is zero, and the normal gradient of the transport variables is zero.

For lateral open boundaries either a specified value or a zero gradient can be given. For specified values, the boundary conditions are imposed by applying the specified concentrations for calculation of the boundary flux. For a zero gradient condition, the concentration at the boundary is assumed to be identical to the concentration at the adjacent interior cell.

3.5 Time stepping procedure

The solution is determined at a sequence of discrete times

$$t^k = t^0 + k\Delta t_{overall} \qquad k = 0, 1, 2, 3 \ldots \tag{3.28}$$

where $\Delta t_{overall}$ is the overall time step interval. The time steps for the hydrodynamic (flow) calculations and the advection-dispersion (transport) calculations are dynamic. The time step procedure is illustrated in Figure 3.2.

For the advection-dispersion (AD) calculations the new time step interval, Δt_{AD}, is determined using the following procedure

$$\Delta t_{AD}^{*} = C_{max} min\left(\frac{\Delta l}{\left(\sqrt{gh_i} + |u_i|\right) + \left(\sqrt{gh_i} + |v_i|\right)}\right) \tag{3.29}$$

$$\Delta t_{AD}^{**} = min\left(max\left(\Delta t_{AD}^{*}, \Delta t_{AD,min}\right), \Delta t_{AD,max}\right) \tag{3.30}$$

$$\Delta t_{AD} = \frac{t^k - t_{AD}}{int\left(\frac{(t^k - t_{AD})}{\Delta t_{AD}^{**}}\right) + 1} \tag{3.31}$$

Here t_{AD} is the actual time for the advection-dispersion calculations, where $t^{k-1} < t_{AD} \leq t^k$. $\Delta t_{AD,min}$ and $\Delta t_{AD,max}$ are the minimum and maximum time step intervals, respectively, and int is the whole number of $(t^k - t_{AD})/\Delta t_{AD}^{**}$. This procedure secures that the time steps for the advection-dispersion calculations are synchronized at the overall discrete time steps.

For the hydrodynamic (HD) calculations the new time step interval, Δt_{HD}, is determined using the following procedure

$$\Delta t_{HD}^{*} = C_{max} min\left(\frac{\Delta l}{|u_i| + |v_i|}\right) \tag{3.32}$$

$$\Delta t_{HD}^{**} = min\left(max\left(\Delta t_{HD}^{*}, \Delta t_{HD,min}\right), \Delta t_{HD,max}\right) \tag{3.33}$$

$$\Delta t_{HD} = \frac{(t_{AD} + \Delta t_{AD}) - t_{HD}}{int\left(\frac{\left((t_{AD} + \Delta t_{AD}) - t_{HD}\right)}{\Delta t_{HD}^{**}}\right) + 1} \tag{3.34}$$

Here t_{HD} is the actual time for the hydrodynamic calculations, where $t_{AD} < t_{HD} \leq t_{AD} + \Delta t_{AD}$. $\Delta t_{HD,min}$ and $\Delta t_{HD,max}$ are the minimum and maximum time step intervals, respectively. This procedure secures that the time steps for the hydrodynamic calculations are synchronized at the advection-dispersion time steps.

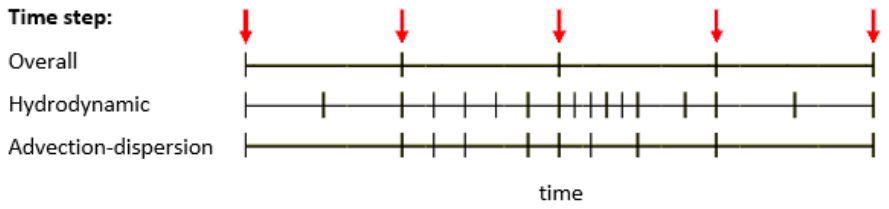

Figure 3.2 Time stepping procedure

4 Physics

4.1 Fluid properties

The rheological properties of a non-Newtonian fluid are driven by the complex interaction of a fluid's chemical and material composition. Key composition properties include the particle size distribution (e.g. percent fines), solids concentration, water content, chemical composition, and mineralogy such as the presence of clay minerals.

The Bingham rheological model is well suited for homogenous fluid mixtures with high concentrations of debris or fine particles (e.g. mudflows, hyper-concentrations of fine sand, silt, and clay-size sediment) and other material types such as oils. The approach is to add a fluid dependent flow resistance to the standard flow momentum equations.

Naef et al. (2006) defines a number of formulations for calculating flow resistance relations and the flow resistance term. The current implementation includes a 'Full Bingham' relation, which in addition allows for applying simpler resistance formulations which excludes the Bingham viscosity term (e.g. the 'Turbulent and Yield' relation as defined in Naef et al (2006)).

The full Bingham flow resistance relation determines the shear stress, τ_0, from the following third order equation (see Naef et al, 2006)

$$2\tau_0^3 - 3\left(\tau_y + 2\frac{\mu_B|\boldsymbol{u}|}{h}\right)\tau_0^2 + \tau_y^3 = 0 \tag{4.1}$$

where $\boldsymbol{u} = (u, v)$ is the depth-integrated flow velocity, h is the fluid depth, τ_y is the yield stress and μ_B is the Bingham fluid viscosity. The resistance terms can then be written

$$\frac{\tau_{fx}}{\rho_0} = \frac{\tau_0}{\rho_0}\frac{u}{|\boldsymbol{u}|} \qquad \frac{\tau_{fy}}{\rho_0} = \frac{\tau_0}{\rho_0}\frac{v}{|\boldsymbol{u}|} \tag{4.2}$$

4.2 Eddy viscosity

In some applications a constant eddy viscosity can be used for the horizontal eddy viscosity. Alternatively, Smagorinsky (1963) proposed to express sub-grid scale transports by an effective eddy viscosity related to a characteristic length scale. The subgrid scale eddy viscosity is given by

$$\nu = c_s^2 l^2 \sqrt{2\left(S_{xx}S_{xx} + 2S_{xy}S_{xy} + S_{yy}S_{yy}\right)} \tag{4.3}$$

where c_s is a constant, l is a characteristic length and the deformation rate is given by

$$S_{xx} = \frac{\partial u}{\partial x} \quad S_{xy} = \frac{1}{2}\left(\frac{\partial u}{\partial y} + \frac{\partial v}{\partial x}\right) \quad S_{yy} = \frac{\partial v}{\partial y} \tag{4.4}$$

For more details on this formulation, the reader is referred to Lilly (1967), Leonard (1974), Aupoix (1984), and Horiuti (1987).

4.3 Bed resistance

The stress due to friction at the bed, $\boldsymbol{\tau}_f = (\tau_{fx}, \tau_{fy})$ is determined by a quadratic friction law

$$\boldsymbol{\tau}_f = \rho_0 c_{fb} \boldsymbol{u}|\boldsymbol{u}| \tag{4.5}$$

where c_{fb} is the drag coefficient, and, $\boldsymbol{u} = (u, v)$ is the depth-averaged flow velocity. The drag coefficient is determined from the Chezy number, C, or the Manning number, M

$$c_{fb} = \frac{g}{C^2} \tag{4.6}$$

$$c_{fb} = \frac{g}{(Mh^{1/6})^2} \tag{4.7}$$

The increase in bed resistance felt by the current due to the presence of waves can be taken into account by calculating a corrected Manning number, M, given the grain diameter and the relative density of the bed material. Here the model for the wave boundary layer in combined wave-current motion proposed by Fredsøe (1994) is applied. For a detailed description of the wave induced bed resistance see also Jones et. al (2014).

4.4 Vegetation

The vegetation structure is modelled as rigid or flexible stems with stem diameter, d_s, or as flexible blades (leaves) with blade width, w_b, and blade thickness, t_b. The height of the vegetation is h_v.

The effect of the vegetation on the flow characteristics is modelled by inclusion of the following drag force in the depth integrated momentum equations

$$\boldsymbol{F}_v = \frac{1}{2} C_D h_v^* b_v \boldsymbol{N_v} \boldsymbol{u}_v |\boldsymbol{u}_v| \tag{4.8}$$

where C_D is the drag coefficient, b_v is the plant size, N_v is the vegetation density and $\boldsymbol{u}_v$ is the apparent velocity vector in the vegetation region. h_v^* is given as $h_v^* = min(h_v, h)$,, where h is the water depth. The plant size is either the stem diameter or the blade width. The vegetation density is the number of plants per unit area. Stone and Chen (2002) proposed the following expression for the apparent velocity

$$\boldsymbol{u}_v = \left(\frac{h_v}{h}\right)^p \boldsymbol{u} \tag{4.9}$$

where $\boldsymbol{u}$ is the flow velocity vector and p=1/2.

For rigid stems a layered approach can be used to take into account the vertical variation of the vegetation. The drag coefficient, $C_{D,i}$, the stem diameter, $d_{s,i}$, the vegetation height, $h_{v,i}$, and the vegetation density, $N_{v,i}$, are then specified for each vertical layer, i. The vegetation height is the distance from the bed to the top of the vegetation layer. The dissipation term due to vegetation is then determined as

$$\boldsymbol{F}_v = \left(\sum_{i=1}^{nlayers} \frac{1}{2} C_{D,i} d_{s,i} (h^*_{v,i} - h^*_{v,i-1}) N_{v,i} \right) \boldsymbol{u}_v |\boldsymbol{u}_v| \tag{4.10}$$

where $h_{v,0} = 0$.

The reduction of the drag due to flexibility of the vegetation is taken into account using the approach by Luhar and Nepf (2011, 2013). They suggested the use of a deflected height, h_d, and an effective length, l_e. The effective length is defined as the length of a rigid vertical plant that generates the same drag as the total length of a flexible plant. The deflected height and the effective length are given by

$$\frac{h_d}{h_v} = 1 - \frac{1 - Ca^{-1/4}}{1 + Ca^{-3/5}(4 + B^{3/5}) + Ca^{-2}(8 + B^2)} \tag{4.11}$$

$$\frac{l_e}{h_v} = 1 - \frac{1 - 0.9Ca^{-1/3}}{1 + Ca^{-3/2}(8 + B^{3/2})} \tag{4.12}$$

where *Ca* is the Cauchy number and *B* is the buoyancy parameter

$$Ca = \frac{\rho A |\boldsymbol{u}_v|^2}{EI/h_v^2} \qquad B = \frac{(\rho - \rho_v) g V_p}{EI/h_v^2} \tag{4.13}$$

Here g is the gravitational acceleration, ρ is the density of water, ρ_v is the density of the plant, E is the elastic modulus for the plant, A is the frontal area, V_p is the volume of the plant element and I is the second moment of the area. For a circular stem

$$A = d_s h_v \qquad V_p = d_s^2 h_v / 4 \qquad I = \pi d_s^4 / 64 \tag{4.14}$$

and for a blade

$$A = w_b h_v \qquad V_p = w_b t_b h_v \qquad I = w_b t_b^3 / 12 \tag{4.15}$$

The flexibility is taken into account by using h_d instead of h_v in Eq. (4.8) and (4.9) and introducing a factor l_e/h_d in Eq. (4.8).

4.5 Wind forcing

In areas not covered by ice the surface stress, $\boldsymbol{\tau}_s = (\tau_{sx}, \tau_{sy})$, is determined by the winds above the surface. The stress is given by the following empirical relation

$$\boldsymbol{\tau}_s = \rho_a c_d \boldsymbol{u}_w |\boldsymbol{u}_w| \tag{4.16}$$

where ρ_a is the density of air, c_d is the drag coefficient of air, and $\boldsymbol{u}_w = (u_w, v_w)$ is the wind speed 10 m above the sea surface.

The drag coefficient can either be a constant value or depend on the wind speed. The empirical formula proposed by Wu (1980, 1994) is used for the parameterization of the drag coefficient

$$c_d = \begin{cases} c_a & W_{10} < W_a \\ c_a + \dfrac{c_b - c_a}{W_b - W_a}(W_{10} - W_a) & W_a \le W_{10} < W_b \\ c_b & W_{10} \ge W_b \end{cases} \quad (4.17)$$

where c_a, c_b, W_a and W_b are empirical factors and W_{10} is the wind velocity 10 m above the sea surface. The default values for the empirical factors are $c_a = 1.255 \cdot 10^{-3}$, $c_b = 2.425 \cdot 10^{-3}$, $W_a = 7m/s$ and $W_b = 25m/s$. These give generally good results for open sea applications. Field measurements of the drag coefficient collected over lakes indicate that the drag coefficient is larger than open ocean data. For a detailed description of the drag coefficient see Geernaert and Plant (1990).

4.6 Ice coverage

It is possible to take into account the effects of ice coverage on the flow field.

In areas where the sea is covered by ice the wind stress is excluded. Instead, the surface stress is caused by the ice roughness. The stress due to friction at the surface, $\boldsymbol{\tau}_f = (\tau_{fx}, \tau_{fy})$, is determined by a quadratic friction law

$$\boldsymbol{\tau}_f = \rho_0 c_{fs} \boldsymbol{u}|\boldsymbol{u}| \quad (4.18)$$

where c_{fs} is the drag coefficient and $\boldsymbol{u} = (u, v)$ is the depth-averaged flow velocity. The drag coefficient is determined from the Manning number, M

$$c_{fs} = \frac{g}{(Mh^{1/6})^2} \quad (4.19)$$

The Manning number is estimated from the ice roughness length, k_s, through

$$M = \frac{25.4}{k_s^{1/6}} \quad (4.20)$$

If ice thickness is specified, the water level is supressed by ρ_{ice}/ρ_{water} of the ice thickness, where $\rho_{ice} = 971\ kg/m^3$ and ρ_{water} is the actual density of the water.

4.7 Tidal potential

The tidal potential is a force, generated by the variations in gravity due to the relative motion of the earth, the moon and the sun that act throughout the computational domain. The forcing is expanded in frequency space and the potential considered as the sum of a number of terms each representing different tidal constituents. The forcing is implemented as a so-called equilibrium tide, which can be seen as the elevation that theoretically would occur, provided the earth was covered with water. The forcing enters the momentum equations as an additional term representing the gradient of the equilibrium tidal elevations, such that the elevation η can be seen as the sum of the actual elevation and the equilibrium tidal potential.

$$\eta = \eta_{actual} + \eta_T \quad (4.21)$$

The equilibrium tidal potential η_T is given as

$$\eta_T = \sum_i e_i H_i f_i L_i cos\left(2\pi \frac{t}{T_i} + b_i + i_0 x\right) \quad (4.22)$$

where η_T is the equilibrium tidal potential, i refers to constituent number (note that the constituents here are numbered sequentially), e_i is a correction for earth tides based on Love numbers, H_i, is the amplitude, f_i, is a nodal factor, L_i, is given below, t is time, T_i, is the period of the constituent, b_i, is the phase and x is the longitude of the actual position.

The phase b is based on the motion of the moon and the sun relative to the earth and can be given by

$$b_i = (i_1 - i_0)s + (i_2 - i_0)h + i_3 p + i_4 N + i_5 p_s + u_i sin(N) \quad (4.23)$$

where i_0 is the species, i_1 to i_5 are Doodson numbers, u is a nodal modulation factor (see Table 4.2) and the astronomical arguments s, h, p, N and P_s are given in Table 4.1.

Table 4.1 Astronomical arguments (Pugh, 1987)

Mean longitude of the moon	s	*277.02+481267.89T+0.0011T²*
Mean longitude of the sun	h	*280.19+36000.77T+0.0003T²*
Longitude of lunar perigee	p	*334.39+4069.04T-0.0103T²*
Longitude of lunar ascending node	N	*259.16-1934.14T+0.0021T²*
Longitude of perihelion	p_s	*281.22+1.72T+0.0005T²*

In Table 4.1 the time, T, is in Julian century from January 1 1900 UTC, thus $T = (365(y - 1900) + (d - 1) + i)/36525$ and $i = int(y - 1901)/4)$, y is year and d is day number

L depends on species number i_0 and latitude ϕ as

$$i_0 = 0\text{: } L = 3sin^2(\phi) - 1$$
$$i_0 = 1\text{: } L = \sin(2\phi)$$
$$i_0 = 2\text{: } L = cos^2(\phi)$$

The nodal factor f_i represents modulations to the harmonic analysis and can for some constituents be given as shown in Table 4.2.

Table 4.2 Nodal modulation terms (Pugh, 1987)

Symbol	f_i	u_i
M_m	*1.000 - 0.130 cos(N)*	*0*
M_f	*1.043 + 0.414 cos(N)*	*-23.7 sin(N)*
Q_1, O_1	*1.009 + 0.187 cos(N)*	*10.8 sin(N)*
K_1	*1.006 + 0.115 cos(N)*	*-8.9 sin(N)*
$2N_2$, μ_2, ν_2, N_2, M_2	*1.000 - 0.037 cos(N)*	*-2.1 sin(N)*
K_2	*1.024 + 0.286 cos(N)*	*-17.7 sin(N)*

4.8 Precipitation and evaporation

In applications where the rainfall is important for the flow, the precipitation rate, $\hat{P}$, can be specified. When heat exchange from the atmosphere is included, the evaporation rate is defined as

$$\hat{E} = \begin{cases} \frac{q_v}{\rho_0 l_v} & q_v > 0 \\ 0 & q_v \leq 0 \end{cases} \tag{4.24}$$

where q_v is the latent heat flux (see section 4.10.1) and l_v is the latent heat of vaporization of water.

Precipitation and evaporation are implemented as a simple source (see section 4.9) in all elements in the computational domain. The discharge in element i is calculated as

$$Q_i = A_i\left(\hat{P} - \hat{E}\right) \tag{4.25}$$

where A_i is the area of the element.

For the transport equations for temperature and salinity the water precipitated and evaporated is assumed to be fresh water at the ambient water temperature (the temperature in element i). For the transport equations for a scalar quantity the concentration is assumed to be the ambient concentration. For precipitation it is also possible to specify the temperature and the concentration of the water flowing into the computation domain.

4.9 Infiltration

The effect of infiltration may be important in cases of flooding scenarios on otherwise dry land. It is possible to account for this in one of two ways: by net infiltration rates or by constant infiltration with capacity.

Infiltration is implemented as a simple source (see section 4.9) in all elements in the computational domain. The discharge in element i is calculated as

$$Q_i = -A_i Q_{net} \tag{4.26}$$

where A_i is the area of the element and Q_{net} is the net infiltration rate.

For the transport equations for temperature and salinity the water infiltration is assumed to be fresh water at the ambient water temperature (the temperature in element i). For the transport equations for a scalar quantity the concentration is be assumed to the ambient concentration. For positive discharge it is also possible to specify the temperature and the concentration of the water flowing into the computation domain.

4.9.1 Net infiltration rates

The net infiltration rate is defined directly. When using net infiltration rate an unsaturated zone is never specified and thus has no capacity limits, so the specified infiltration rates will always be fully effectuated if there is enough water available in the element.

4.9.2 Constant infiltration with capacity

Constant infiltration with capacity describes the infiltration from the free surface zone to the unsaturated zone and from the unsaturated zone to the saturated zone by a simplified model (se Figure 4.1). The model assumes the following:

- The unsaturated zone is modelled as an infiltration zone with constant porosity over the full depth of the zone.
- The flow between the free surface zone and the infiltration zone is based on a constant flow rate, Q_i.
- The flow between the saturated and unsaturated zone is modelled as a leakage having a constant flow rate, Q_l.

The simplified model described above is solved through a one-dimensional continuity equation for the unsaturated zone. Feedback from the infiltration and leakage to the two-dimensional horizontal hydrodynamic calculations is based solely on changes to the depth of the free surface zone – the water depth.

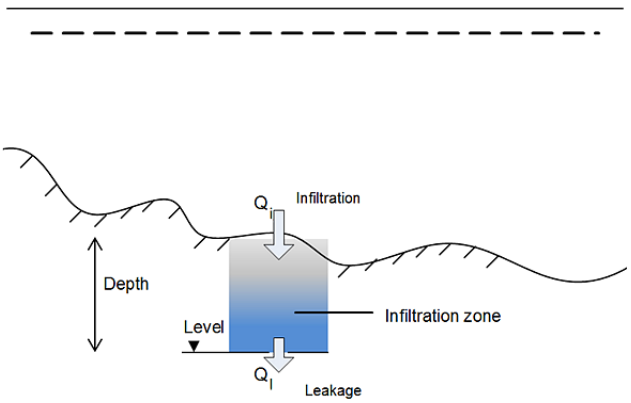

Figure 4.1 Illustration of infiltration process

4.10 Wave Radiation

The radiation stress is the depth-integrated excess momentum flux due to the breaking of the short period waves. The radiation stresses act as driving forces for the mean flow and can be used to calculate wave setup and wave induced currents.

$$F_x = \frac{1}{\rho_0 h}\left(\frac{\partial S_{xx}}{\partial x} + \frac{\partial S_{xy}}{\partial y}\right) \qquad F_y = \frac{1}{\rho_0 h}\left(\frac{\partial S_{xy}}{\partial x} + \frac{\partial S_{yy}}{\partial y}\right) \qquad F_z = 0 \tag{4.27}$$

where S_{xx}, S_{xy}, and S_{yy} are components of the second order radiation stress tensor.

4.11 Sources

There are three types of sources

- Simple source
- Standard source

- Connected source

For a simple source the discharge, Q, is specified. If the source is located in element i with the area A_i the following source term is added to the discrete continuity equation

$$S_i = \frac{Q}{A_i} \tag{4.28}$$

A source where the discharge is negative is also called a sink. For a simple source the mass enters the flow without momentum. The mass will therefore have to be accelerated, and this may cause a drop in the local velocity. For a standard source a source of momentum is also included. The following terms are added to the discrete momentum equations

$$F_{x,i} = u_s \frac{Q}{A_i} \qquad F_{y,i} = v_s \frac{Q}{A_i} \tag{4.29}$$

where u_s and v_s are the source velocities. The contribution to the momentum equation is only taken into account when the magnitude of the source is positive (water is discharge into the ambient). A connected source is a standard source where the magnitude of the discharge is obtained as the magnitude of the discharge specified for source which the source is connected to, but with opposite sign.

For the transport equations a source term is also added to the discrete equation. The source term is S_i times a value for the transported variable. This can be a specified value or the value in the element where the source is located plus an excess value.

4.12 Heat exchange

The heat exchange with the atmosphere is calculated on basis of the four physical processes

- Latent heat flux (or the heat loss due to vaporisation)
- Sensible heat flux (or the heat flux due to convection)
- Net short wave radiation
- Net long wave radiation

The source term is given by

$$\widehat{H} = q_v + q_c + q_{sr,net} + q_{lr,net} \tag{4.30}$$

The calculation of the latent heat flux, q_v, sensible heat flux, q_c,, net short wave radiation, $q_{sr,net}$, and net long wave radiation, $q_{lr,net}$, as described in the following sections.

In areas covered by ice the heat exchange with the atmosphere is excluded.

The heat in the water can also interact with the ground due to ground heat conduction.

4.12.1 Vaporisation

Dalton's law yields the following relationship for the vaporative heat loss (or latent flux), see Sahlberg, 1984

$$q_v = LC_e(a_1 + b_1 W_{2m})(Q_{water} - Q_{air}) \tag{4.31}$$

where $L = 2.5 \cdot 10^6 J/kg$ is the latent heat vaporisation (in the literature $L = 2.5 \cdot 10^6 - 2300 T_{water}$ is commonly used, where T_{water} is the temperature of the water); $C_e = 1.32 \cdot 10^{-3}$ is the moisture transfer coefficient (or Dalton number); W_{2m} is the wind speed 2 m above the sea surface; Q_{water} is the water vapour density close to the surface; Q_{air} is the water vapour density in the atmosphere; a_1 and b_1 are user specified constants. The default values are $a_1 = 0.5$ and $b_1 = 0.9$.

Measurements of Q_{water} and Q_{air} are not directly available but the vapour density can be related to the vapour pressure as

$$Q_i = \frac{0.2167}{T_i + T_k} e_i \tag{4.32}$$

in which subscript i refers to both water and air. The vapour pressure close to the sea, e_{water}, can be expressed in terms of the water temperature assuming that the air close to the surface is saturated and has the same temperature as the water

$$e_{water} = 6.11 \exp\left(k\left(\frac{1}{T_k} - \frac{1}{T_{water} + T_k}\right)\right) \tag{4.33}$$

where $k = 5418°K$ and $T_k = 273.15°K$ is the temperature at $0°C$. Similarly, the vapour pressure of the air, e_{air}, can be expressed in terms of the air temperature and the relative humidity, R

$$e_{air} = R \cdot 6.11 \exp\left(k\left(\frac{1}{T_k} - \frac{1}{T_{air} + T_k}\right)\right) \tag{4.34}$$

Replacing Q_{water} and Q_{air} with these expressions the latent heat can be written as

$$q_v = -P_v(a_1 + b_1 W_{2m})\left(\frac{\exp\left(k\left(\frac{1}{T_k} - \frac{1}{T_{water} + T_k}\right)\right)}{T_{water} + T_k} - \frac{\mathrm{R} \cdot \exp\left(k\left(\frac{1}{T_k} - \frac{1}{T_{air} + T_k}\right)\right)}{T_{air} + T_k}\right) \tag{4.35}$$

where all constants have been included in a new latent constant $P_v = 4370 J°K/m^3$. During cooling of the surface the latent heat loss has a major effect with typical values up to 100 W/m^2.

The wind speed, W_2, 2 m above the sea surface is calculated from the wind speed, W_{10}, 10 m above the sea surface. Assuming a logarithmic profile the wind speed, $u(z)$ at a distance z above the sea surface is given by

$$u(z) = \frac{u_*}{\kappa} log\left(\frac{z}{z_0}\right) \tag{4.36}$$

where u_* is the wind friction velocity, z_0 is the sea roughness and $\kappa = 0.4$ is von Karman's constant. $u_*$and z_0 are given by

$$z_0 = z_{Charnock}\frac{u_*}{g} \tag{4.37}$$

$$u_* = \frac{\kappa u(z)}{log\left(\frac{z}{z_0}\right)} \tag{4.38}$$

where $z_{Charnock}$ is the Charnock parameter. The default value is $z_{Charnock} = 0.014$. The wind speed, W_2, is then calculated from the wind speed, W_{10}, by first solving Eq. 4.37 and Eq. 4.38 iteratively for z_0 with $z = 10m$ and $u(z) = W_{10}$. Then W_2 is given by

$$\begin{aligned} W_2 &= W_{10}\frac{log\left(\frac{2}{z_0}\right)}{log\left(\frac{10}{z_0}\right)} && W_{10} > 0.5m/s \\ W_2 &= W_{10} && W_{10} \le 0.5m/s \end{aligned} \tag{4.39}$$

The heat loss due to vaporization occurs both by wind driven forced convection and by free convection. The effect of free convection is taken into account by the parameter a_1 in Eq. 4.31. The free convection is also taken into account by introducing a critical wind speed $W_{critical}$ so that the wind speed used in Eq. 4.39 is obtained as $W_{10} = \max(W_{10}, W_{critical})$. The default value for the critical wind speed is 2 m/s.

4.12.2 Convection

The sensible heat flux, q_c, measured in W/m^2 (or the heat flux due to convection) depends on the type of boundary layer between the sea surface and the atmosphere. Generally, this boundary layer is turbulent implying the following relationship

$$q_c = \begin{cases} \rho_{air} c_{air} c_{heating} W_{10}(T_{air} - T_{water}) & T_{air} \ge T_{water} \\ \rho_{air} c_{air} c_{cooling} W_{10}(T_{air} - T_{water}) & T_{air} < T_{water} \end{cases} \tag{4.40}$$

where ρ_{air} is the air density $1.225\ kg/m^3$; $c_{air} = 1007\ J/(kg \cdot °K)$ is the specific heat of air; $c_{heating} = 0.0011$ and $c_{cooling} = 0.0011$, respectively, is the sensible transfer coefficient (or Stanton number) for heating and cooling (see Kantha and Clayson, 2000); W_{10} is the wind speed $10\ m$ above the sea surface; T_{water} is the temperature at the sea surface; T_{air} is the temperature of the air.

The convective heat flux typically varies between 0 and $100\ W/m^2$.

The heat loss due to convection occurs both by wind driven forced convection and by free convection. The free convection is taken into account by introducing a critical wind speed $W_{critical}$ so that the wind speed used in Eq. 4.40 is obtained as $W_{10} = \max(W_{10}, W_{critical})$. The default value for the critical wind speed is $2\ m/s$.

4.12.3 Short wave radiation

Radiation from the sun consists of electromagnetic waves with wave lengths varying from $1{,}000$ to $30{,}000$ Å. Most of this is absorbed in the ozone layer, leaving only a fraction of the energy to reach the surface of the Earth. Furthermore, the spectrum changes when

sunrays pass through the atmosphere. Most of the infrared and ultraviolet compound is absorbed such that the solar radiation on the Earth mainly consists of light with wave lengths between $4{,}000$ and $9{,}000$ Å. This radiation is normally termed short wave radiation. The intensity depends on the distance to the sun, declination angle and latitude, extraterrestrial radiation and the cloudiness and amount of water vapour in the atmosphere (see Iqbal, 1983)

The eccentricity in the solar orbit, E_0, is given by

$$E_0 = \left(\frac{r_0}{r}\right)^2 = 1.000110 + 0.034221\cos(\Gamma) + 0.001280\sin(\Gamma) + 0.000719\cos(2\Gamma) + 0.000077\sin(2\Gamma) \quad (4.41)$$

where r_0 is the mean distance to the sun, r is the actual distance and the day angle Γ is defined by

$$\Gamma = \frac{2\pi(d_n - 1)}{356} \quad (4.42)$$

and d_n is the Julian day of the year.

The daily rotation of the Earth around the polar axes contributes to changes in the solar radiation. The seasonal radiation is governed by the declination angle, δ, measured in *rad* which can be expressed by

$$\delta = 0.006918 - 0.399912\cos(\Gamma) + 0.07257\sin(\Gamma) - 0.006758\cos(2\Gamma) + 0.000907\sin(2\Gamma) - 0.002697\cos(3\Gamma) + 0.00148\sin(3\Gamma) \quad (4.43)$$

The day length, n_d, varies with δ. For a given latitude, ϕ, (positive on the northern hemisphere) the day length is given by

$$n_d = \frac{24}{\pi}\arccos\big(-\tan(\phi)\tan(\delta)\big) \quad (4.44)$$

and the sunrise angle, ω_{sr}, and the sunset angle ω_{ss} are

$$\omega_{sr} = \arccos\big(-\tan(\phi)\tan(\delta)\big) \quad and \quad \omega_{ss} = -\omega_{ss} \quad (4.45)$$

The intensity of short wave radiation on the surface parallel to the surface of the Earth changes with the angle of incidence. The highest intensity is in zenith and the lowest during sunrise and sunset. Integrated over one day the extraterrestrial intensity, H_0, measured in $MJ/m^2/day$ in short wave radiation on the surface can be derived as

$$H_0 = \frac{24}{\pi} q_{sc} E_0 \cos(\phi)\cos(\delta)\big(\sin(\omega_{sr}) - \omega_{sr}\cos(\omega_{sr})\big) \quad (4.46)$$

where $q_{sc} = 4.9212\ MJ/m^2/h$ is the solar constant.

For determination of daily radiation under cloudy skies, H, measured in $MJ/m^2/day$, the following relation is used

$$\frac{H}{H_0} = a_2 + b_2\frac{n}{n_d} \quad (4.47)$$

in which n is the number of sunshine hours and n_d is the maximum number of sunshine hours. a_2 and b_2 are user specified constants. The default values are $a_2 = 0.295$ and $b_2 =$

0.371. The user-specified clearness coefficient corresponds to n/n_d. Thus the solar radiation, q_s, measured in W/m^2 can be expressed as

$$q_s = \left(\frac{H}{H_0}\right) q_0 \left(a_3 + b_3 \cos(\omega_i)\right) \frac{10^6}{3600} \tag{4.48}$$

where

$$a_3 = 0.4090 + 0.5016 \sin\left(\omega_{sr} - \frac{\pi}{3}\right) \tag{4.49}$$

$$b_3 = 0.6609 + 0.4767 \sin\left(\omega_{sr} - \frac{\pi}{3}\right) \tag{4.50}$$

The extraterrestrial intensity, q_0 $(MJ/m^2/h)$ and the hour angle ω_i is given by

$$q_0 = q_{sc} E_0 \left(\sin(\phi)\sin(\delta) + \frac{24}{\pi}\cos(\phi)\cos(\delta)\cos(\omega_i)\right) \tag{4.51}$$

$$\omega_i = \frac{\pi}{12}\left(12 + \Delta t_{displacement} + \frac{4}{60}(L_S - L_E) - \frac{E_t}{60} - t_{local}\right) \tag{4.52}$$

$\Delta t_{displacement}$ is the displacement hours due to summer time and the time meridian L_S is the standard longitude for the time zone. $\Delta t_{displacement}$ and L_S are user specified constants. The default values are $\Delta t_{displacement} = 0\ h$ and $L_S = 0\ deg$. L_E is the local longitude in degrees. $E_t\ (s)$ is the discrepancy in time due to solar orbit and is varying during the year. It is given by

$$\begin{aligned} E_t = \big(&0.000075 + 0.001868\cos(\Gamma) - 0.032077\sin(\Gamma) - 0.014615\cos(2\Gamma) \\ &- 0.04089\sin(2\Gamma)\big) \cdot 229.18 \end{aligned} \tag{4.53}$$

Finally, t_{local} is the local time in hours.

Solar radiation that impinges on the sea surface does not all penetrate the water surface. Parts are reflected back and are lost unless they are backscattered from the surrounding atmosphere. This reflection of solar energy is termed the albedo. The amount of energy, which is lost due to albedo, depends on the angle of incidence and angle of refraction. For a smooth sea the reflection can be expressed as

$$\alpha = \frac{1}{2}\left(\frac{\sin^2(i-r)}{\sin^2(i+r)} + \frac{\tan^2(i-r)}{\tan^2(i+r)}\right) \tag{4.54}$$

Where i is the angle of incidence, r the refraction angle and α the reflection coefficient, which typically varies from 5 to 40 %. α can be approximated using

$$\alpha = \begin{cases} \dfrac{altitude}{5} 0.48 & altitude < 5 \\ \dfrac{30 - altitude}{25}(0.48 - 0.05) & 5 \le altitude \le 30 \\ 0.05 & altitude > 30 \end{cases} \tag{4.55}$$

where the altitude in degrees is given by

$$altitude = 90 - \left(\frac{180}{\pi}\arccos\left(\sin(\delta)\sin(\phi) + \cos(\delta)\cos(\phi)\cos(\omega_i)\right)\right) \quad (4.56)$$

Thus the net short wave radiation, $q_{st,net}$ (W/m^2), can possibly be expressed as

$$q_{sr,net} = (1 - \alpha)q_s \quad (4.57)$$

The net short wave radiation, $q_{sr,net}$, can be calculated using empirical formulae as described above. Alternatively, the net short wave radiation can be calculated using Eq. 4.57, where the solar radiation, q_s, is specified by the user or the net short wave radiation, $q_{sr,net}$, can be given by the user.

4.12.4 Long wave radiation

A body or a surface emits electromagnetic energy at all wavelengths of the spectrum. The long wave radiation consists of waves with wavelengths between $9{,}000$ and $25{,}000$ Å. The radiation in this interval is termed infrared radiation and is emitted from the atmosphere and the sea surface. The long wave emittance from the surface to the atmosphere minus the long wave radiation from the atmosphere to the sea surface is called the net long wave radiation and is dependent on the cloudiness, the air temperature, the vapour pressure in the air and the relative humidity. The net outgoing long wave radiation, $q_{lr,net}$, measured in W/m^2 is given by Brunt's equation (See Lind and Falkenmark, 1972)

$$q_{lr,net} = -\sigma_{sb}(T_{air} + T_k)^4\left(a - b\sqrt{e_d}\right)\left(c + d\frac{n}{n_d}\right) \quad (4.58)$$

where e_d is the vapour pressure at dew point temperature measured in mb; n is the number of sunshine hours, n_d is the maximum number of sunshine hours; $\sigma_{sb} = 5.6697 \cdot 10^{-8}\ W/(m^2 \cdot {}^\circ K^4)$ is Stefan Boltzman's constant; T_{air} $({}^\circ C)$ is the air temperature. The coefficients a, b, c and d are given as

$$a = 0.56 \quad b = 0.077\ mb^{-\frac{1}{2}} \quad c = 0.1 \quad d = 0.9 \quad (4.59)$$

The vapour pressure is determined as

$$e_d = 10 \cdot R\ e_{saturated} \quad (4.60)$$

where R is the relative humidity and the saturated vapour pressure, $e_{saturated}$, measured in kPa with 100 % relative humidity in the interval from -51 to 52 $^\circ C$ can be estimated by

$$e_{saturated} = 3.38639 \cdot ((7.38 \cdot 10^{-3} \cdot T_{air} + 0.8072)^8 - 1.9 \cdot 10^{-5}|1.8 \cdot T_{air} + 48| + 1.316 \cdot 10^{-3}) \quad (4.61)$$

The net long wave radiation, $q_{lr,net}$, can be calculated using empirical formulae as described above. Alternatively, the net long wave radiation can be calculated as

$$q_{lr,net} = q_{ar,net} - q_{br} \quad (4.62)$$

where the net incident atmospheric radiation, $q_{ar,net}$, is specified by the user and the back radiation, q_{br}, is given by

$$q_{br} = (1 - r)\varepsilon\sigma_{sb}T_k^4 \quad (4.63)$$

where $r = 0.03$ is the reflection coefficient and $\varepsilon = 0.985$ is the emissivity factor of the atmosphere. The net long wave radiation can also be specified by the user.

4.12.5 Ground heat

The heat conduction at the bed is a function of the difference between the temperature at the bed and at an equilibrium ground temperature which will be some distance below the bed. The heat flux, q_g , through the bed is given by

$$q_d = K_g \frac{(T_g - T_w)}{\Delta z_g} \Delta z \tag{4.64}$$

where K_g (Watt/m/°C) is the thermal conductivity of the bed material (etc. soil, sand or rock), T_g is the ground equilibrium temperature, T_w is the water temperature at the bed/water interface and Δz_g is distance from the bed/ground level to the level where the equilibrium ground temperature is specified.

4.13 Porosity

The main effects of porosity are introduced by additional laminar and turbulent friction terms for describing losses due to flow through a porous structure. In most practical cases the pore sizes are relatively large (typically 0.1m to 1.0m), and the turbulent losses will dominate. The laminar loss term has also been included to allow the simulation of small scale physical model tests.

The flow resistance components $\boldsymbol{F}_p = \left(\boldsymbol{F}_{px}, \boldsymbol{F}_{py}\right)^T$ inside the porous structure are described by the linear and non-linear resistance forces expressed as

$$\boldsymbol{F}_p = ah\tilde{\boldsymbol{u}} + b|\tilde{\boldsymbol{u}}|h\tilde{\boldsymbol{u}} \tag{4.65}$$

where a and b are resistance coefficients accounting for the laminar and turbulent friction loss, respectively, $\tilde{\boldsymbol{u}} = (nu, nv)$ is the filter velocity vector, and the magnitude of the filter velocity is defined by $|\tilde{\boldsymbol{u}}| = \sqrt{\tilde{\boldsymbol{u}} \cdot \tilde{\boldsymbol{u}}}$. a and b are determined by the empirical expressions formulated by Engelund (1953) and van Gent (1995),

$$a = \alpha \frac{(1-n)^2}{n^3} \frac{\vartheta}{D_{50}^2} \tag{4.66}$$

$$b = \beta \frac{(1-n)}{n^3} \frac{1}{D_{50}} \tag{4.67}$$

where n is the porosity, α and β are user specified coefficients, ϑ is the kinematic viscosity and D_{50} is the grain diameter of the porous materials.

In the momentum equations the time derivative terms are multiplied by a factor $(1 + c_m)$ where c_m is the added mass coefficient to take transient interaction between grains and water into account. van Gent (1995) gave c_m as

$$c_m = \gamma \frac{1-n}{n} \tag{4.68}$$

where γ is an empirical coefficient, which takes the value 0.34. For further details the reader is referred to Appendix B.

5 Structures

The horizontal dimension of structures is usually much smaller than the element (cell) sizes used in the computational grid. Therefore, the effect of structures is modeled by a subgrid technique. Six types of structures are included in the model

- Weirs
- Culverts
- Dikes
- Gates
- Piers
- Turbines

In addition, a composite structure can be used. A composite structure is a combination of a number of weirs and culverts.

Weirs, culverts, dikes and gates are defined as line sections. The location in the domain of a line section is given by a number of geo-referenced points which together make up a polyline. This is illustrated in Figure 5.1. The polyline defines the width of the cross section perpendicular to the flow direction. A minimum of two points is required. The polyline is composed of a sequence of line segments. The line segments are straight lines between two successive points. The polyline (line section) in the numerical calculations is defined as a section of element faces. The face is included in the section when the line between the two element centers of the faces crosses one of the line segments. If two faces in a triangular element are part of the same face section, the face section is corrected so that these two faces are excluded from the face section and instead the third face in the triangle is applied. The left and right side of the of the line section is defined by positioning at the start point and looking forward along the line section.

Piers and turbines are defined as points in the domain

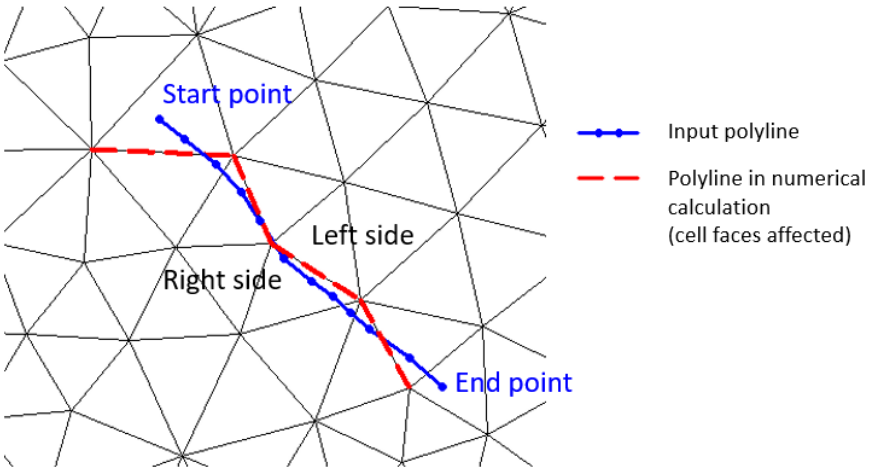

Figure 5.1 The location of a line section.

5.1 Weirs

A weir is defined as a cross (line) section where the total discharge across the cross section is calculated using empirical formulas and distributed along the cross section. In the numerical calculations the cross section is defined as a section of element faces

which is treated as an internal discharge boundary (weak formulation). However, the flux contribution to the continuity equation is corrected to secure mass conservation.

The total discharge is calculated based on the mean water level in the real wet elements to the left and right of the section of faces. The mean level is calculated using the length of the element faces as the weighting factor. Real wet elements are elements where the water depth is larger than the wetting depth. The upstream water level is then the highest of the two water levels and the downstream water level the smallest. The distribution of the calculated total discharge along the section faces can be specified in two ways

- Uniform
- Non-uniform

The discharge is in both cases distributed to the faces for which the element to the left and right of the face are both a wet element and else the discharge is distributed to the faces for which the upstream elements are wet elements. When non-uniform distribution is applied the discharge will be distributed as it would have been in a uniform flow field with the Manning resistance law applied, i.e. relative to $h^{5/3}$, where h is the total water depth. This distribution is, in most cases, a good approximation. This does not apply if there are very large variations over the bathymetry or the geometry.

When the difference between the upstream and downstream water level for a weir is small the corresponding gradient of the discharge with respect to the water levels is large. This in turn may result in a very rapid flow response to minor changes in the water level upstream and downstream. As a way of controlling this effect an Alpha zero value has been introduced. The Alpha zero value defines the water level difference below which the discharge gradients are suppressed. The default setting is 0.01 meter.

For weirs a valve regulation is applied. Four different valve regulation types are available

- None. No valve regulation applies (flow is not regulated).
- Only Negative Flow. Only flow in negative flow direction is allowed. Valve regulation does not allow flow in positive flow direction and the flow through the structure will be zero in this case.
- Only Positive Flow. Only flow in positive flow direction is allowed. Valve regulation does not allow flow in negative flow direction and the flow through the structure will be zero in this case.
- No Flow. No flow is allowed in the structure. Valve regulation closes completely the structure.

The flow direction is positive when the flow occurs from the right of the line structure to the left (see Figure 5.1)

Three formulas are available for calculation of the discharge through a weir

- Broad Crested Weir formula
- Weir formula 1
- Weir formula 2 (Honma formula)

Broad Crested Weir

For a broad crested weir the shape of the "hole" is described through a level/width table (see Figure 5.2 and Figure 5.3). Levels are defined relative to the datum (starting from the crest or sill level and up). A datum value for the weir may be used to shift the levels by a

constant amount. This is typically used if the weir geometry has been surveyed with respect to a local benchmark.

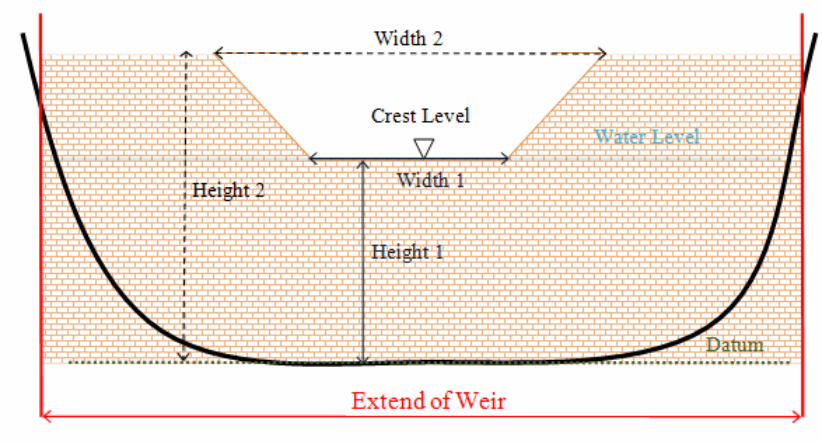

Figure 5.2 Setup definitions of contracted weir.

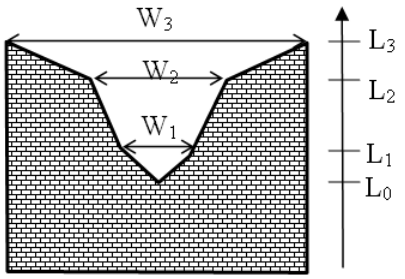

Level	Width
L_0	0
L_1	W_1
L_2	W_2
L_3	W_3

Figure 5.3 Definition sketch for broad crested weir geometry.

The standard formulations for flow over a broad crested weir are established on the basis of the weir geometry and the specified head loss and calibration coefficients. These formulations assume a hydrostatic pressure distribution on the weir crests. Different algorithms are used for drowned flow and free overflow, with an automatic switching between the two.

The energy loss over a weir is given by

$$q = \zeta_t \frac{V_s}{2g} \tag{5.1}$$

where ζ_t is the total head loss coefficient and V_s is the mean cross sectional velocity at the structure. The total head loss coefficient, ζ_t, is composed of entrance, ζ_1, and exit, ζ_2, loss coefficients. The coefficients are generally related to the input parameters for inflow, ζ_{in}, and outflow, ζ_{out}, and the changes in velocity, V, and area, A

$$\zeta_t = \zeta_1 + \zeta_2 = \zeta_{in}\left(\frac{V_1}{V_s}\right) + \zeta_{out}\left(\frac{A_s}{A_2}\right)^2 \tag{5.2}$$

where suffix '1' and '2' represents velocity and area on inflow and outflow side of the structure respectively, and '*s*' represents the velocity and area in the structure itself. However, in the present implementation, upstream and downstream cross sections are not extracted and accordingly, tabulated relations on cross section areas as function of

water levels are not known. Instead, upstream and downstream areas are set to a large number resulting in a full loss contribution from the head loss factors defined

$$\zeta_t = \zeta_1 + \zeta_2 = \zeta_{in} + \zeta_{out} \tag{5.3}$$

Care must be taken when selecting loss coefficients, particularly in situations where both subcritical and supercritical flow conditions occur. When flow conditions change from subcritical to supercritical (or the Froude number, FR, becomes greater than 1), the loss coefficients ζ_{in} and ζ_{out} are modified:

- If FR > 1 for upstream conditions, then $\zeta_{in} = \zeta_{in}/2$
- If FR > 1 for downstream conditions, then $\zeta_{out} = \zeta_{out}/2$

The critical flows are multiplied by the critical flow correction factor, α_c, specified as the free overflow head loss factor. Typically, a value of 1.0 is used.

Weir formula 1

For the Weir formula 1 description the parameters are given by Figure 5.4. The width is perpendicular to the flow direction. Typically, the invert level coincides with the overall datum. Weir formula 1 is based on a standard weir expression, reduced according to the Villemonte formula

$$q = C(\eta_{US} - z_W)^k \left(1 - \frac{\eta_{DS} - z_W}{\eta_{US} - z_W}\right)^{-0.385} W \tag{5.4}$$

where q is the discharge through the structure, W is the width, C is the weir coefficient, k is the weir exponential coefficient, η_{US} is the upstream water level, η_{DS} is the downstream water level and z_w is the weir level (see Figure 5.4). The invert level is the lowest point in the inlet or outlet section respectively.

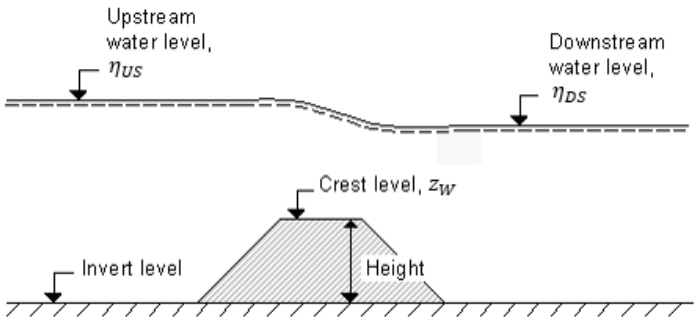

Figure 5.4 Definition sketch for weir flow.

Weir formula 2

For the Weir formula 2 the geometry is given by a crest level and a width. The crest level is taken with respect to the global datum. The width is perpendicular to the flow direction. Weir formula 2 is the Honma formula

$$q = \begin{cases} C_1(\eta_{US} - z_W)\sqrt{\eta_{US} - z_w}\, W & \frac{(\eta_{DS} - z_W)}{\eta_{US}} < \frac{2}{3} \\ C_2(\eta_{DS} - z_W)\sqrt{\eta_{US} - \eta_{DS}} W & \frac{(\eta_{DS} - z_W)}{\eta_{US}} \geq \frac{2}{3} \end{cases} \quad (5.5)$$

where q is the discharge through the structure, W is the width, C_1 and $C_2 = 1.5\sqrt{3}C_1$ are the two weir coefficients, η_{US} is the upstream water level, η_{DS} is the downstream water level and z_W is the weir level (see Figure 5.4).

5.2 Culverts

A culvert can be modelled either as a short or a long culvert.
A short culvert is defined as a cross (line) section where the total discharge across the cross section is calculated using empirical formulas and distributed along the cross section. In the numerical calculations the cross section is defined as a section of element faces which is treated as an internal discharge boundary (weak formulation). However, the flux contribution to the continuity equation is corrected to secure mass conservation.

A long culvert is defined by a longitudinal line as shown in Figure 5.5 where the inlet and outlet location are defined as two extent lines at the ends of the transversal line. The polyline (line section) in the numerical calculations for each of the two extent lines is defined as a section of element faces. A long culvert is treated as two connected area sources where the total discharge is calculated using empirical formulas. For each of the two extent lines, the area is determined at the area of the elements to the right of the section of element faces. At the outlet location it is possible to take into account the contribution to the momentum equation. This contribution is estimated as the discharge multiplied by a velocity. Here the magnitude of the velocity is calculated as the discharge divided by the local total water depth. The direction used for the two extent lines is the direction of the first and last segment of the longitudinal polyline. If the longitidinal polyline only contains one segment (two points), the direction is determined as the direction perpendicular to the line given by the first and last point of the extent line.

For a short culvert the total discharge is calculated based on the mean water level in the real wet elements to the left and right of the section of faces. For a long culvert the total discharge calculated based on the mean water level in the real wet elements to the right of the section of faces for the two extent lines. The mean level is calculated using the length of the element faces as the weighting factor. Real wet elements are elements where the water depth is larger than the wetting depth. The upstream water level is then the highest of the two water levels and the downstream water level the smallest.

The distribution of the calculated total discharge along the section faces can be specified in two ways

- Uniform
- Non-uniform

For a short culvert the discharge is in both cases distributed to the faces for which the element to the left and right of the face are both a wet element and else the discharge is distributed to the faces for which the upstream elements are wet elements. When non-uniform distribution is applied the discharge will be distributed as it would have been in a uniform flow field with the Manning resistance law applied, i.e. relative to $h^{5/3}$, where h is the total water depth. For a long culvert the discharge is in both cases distributed to the faces for which the element to the right of the extent line is a wet element. If no elements are wet the discharge is distributed uniformly to all faces in the section. When non-uniform

distribution is applied the same approach as for short culverts is used. The non-uniform distribution is, in most cases, a good approximation. This does not apply if there are very large variations over the bathymetry or the geometry.

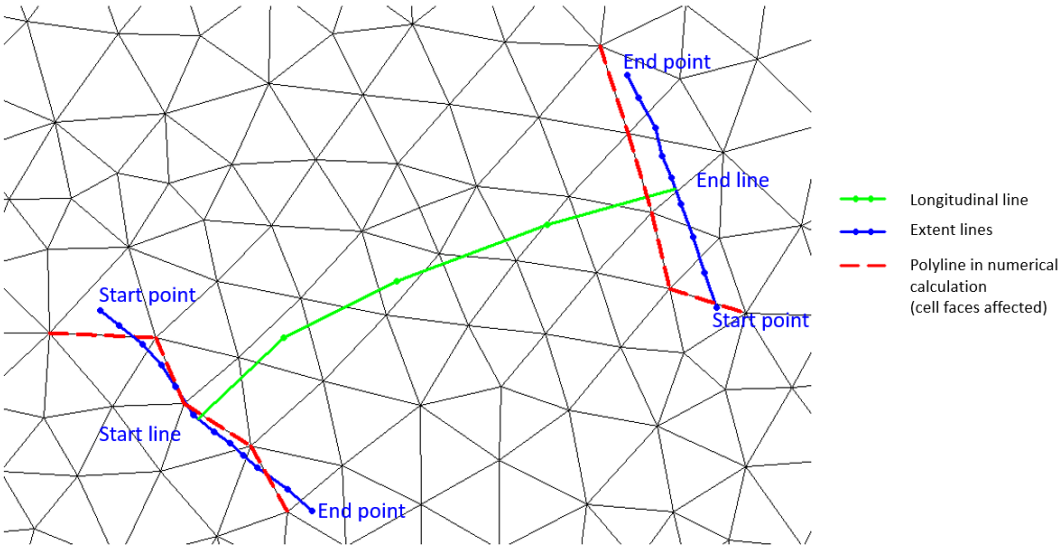

Figure 5.5 Setup definitions for a long culvert.

When the difference between the upstream and downstream water level for both a short and long culvert is small the corresponding gradient of the discharge with respect to the water levels is large. This in turn may result in a very rapid flow response to minor changes in the water level upstream and downstream. As a way of controlling this effect an Alpha zero value has been introduced. The Alpha zero value defines the water level difference below which the discharge gradients are suppressed. The default setting is 0.01 meter.

For both short and long culverts a valve regulation is applied. Four different valve regulation types are available

- None. No valve regulation applies (flow is not regulated).
- Only Negative Flow. Only flow in negative flow direction is allowed. Valve regulation does not allow flow in positive flow direction and the flow through the structure will be zero in this case.
- Only Positive Flow. Only flow in positive flow direction is allowed. Valve regulation does not allow flow in negative flow direction and the flow through the structure will be zero in this case.
- No Flow. No flow is allowed in the structure. Valve regulation closes completely the structure.

For a short culvert the flow direction is positive when the flow occurs from the right of the line structure to the left (see Figure 5.1). For a long culvert the flow direction is positive when flow is from the start line to the end line (Figure 5.5).

The culvert geometry defines the geometrical shape of the active flow area of the culvert, see Figure 5.6. The cross sectional geometry of a culvert can be specified as

- Rectangular. The width and height specify the geometry.
- Circular. The geometry is specified by the diameter.

- Irregular Level-Width Table. The geometry is specified using a level/width table. The Level/Width table defines the culvert shape as a set of corresponding levels and flow widths (see Figure 5.7).

A culvert structure can be modelled as either an open section or a closed section. If set to open the culvert will never run full or partially full, therefore only those flow conditions which represent a free water surface are modelled. When the water level is higher than the soffit the hydraulic parameters are calculated based on a section extended vertically upwards with a width equal to that at the soffit. For example, in the case of a rectangular section the height value is essentially redundant as the cross-section will be modeled as an open section of constant width. A circular culvert is always a treated as a closed section.

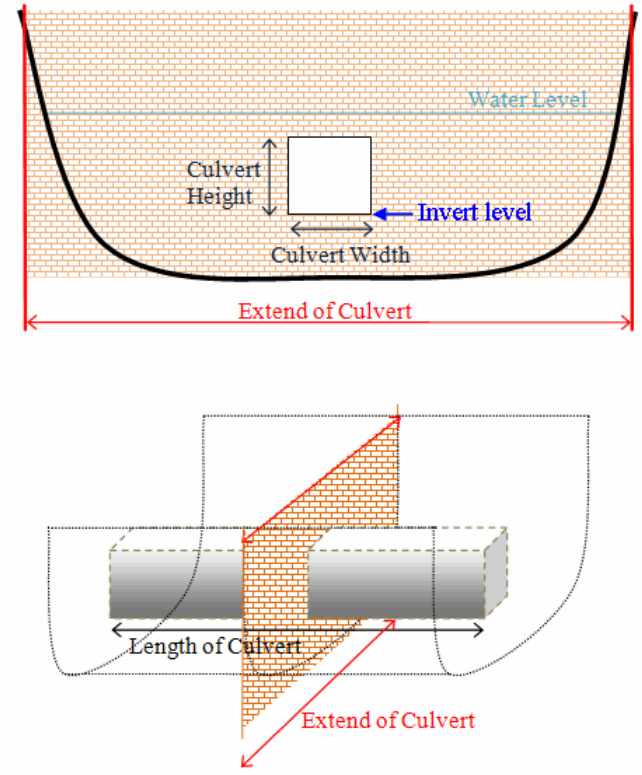

Figure 5.6 Setup definitions of culverts.

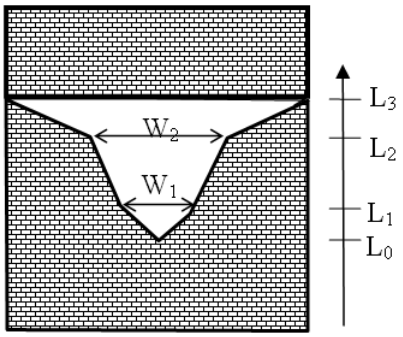

Level	Width
L_0	0
L_1	W_1
L_2	W_2
L_3	W_3

Figure 5.7 Definition sketch for irregular culvert geometry.

The total head loss, ΔH_{loss} through a culvert is given by

$$\Delta H_{loss} = \frac{q^2}{2g}\left(\frac{\zeta_1}{A_{s_1}^2} + \frac{\zeta_f + \zeta_b}{A_{s_A}^2} + \frac{\zeta_2}{A_{s_2}^2}\right) \tag{5.6}$$

where A_{S_1}, A_{S_A} and A_{S_2} are the mean cross section areas along the length of the culvert and q is the discharge, ζ_1 is the entrance or contraction loss coefficient, ζ_2 is the outlet or expansion loss coefficient, ζ_f is the friction loss and ζ_b is the bend loss coefficient. ζ_1 and ζ_2 are calculated by

$$\zeta_1 = \zeta_{in}\left(1 - \frac{A_s}{A_1}\right) \tag{5.7}$$

$$\zeta_2 = \zeta_{out}\left(1 - \frac{A_s}{A_2}\right)^2 \tag{5.8}$$

The upstream and downstream cross section areas, A_1 and A_2 are not processed and extracted in the present implementation and hence, defined as an infinite value. Contraction and expansion losses are therefore assumed to be applied in full using the defined inflow and outflow loss coefficients, ζ_{in} and ζ_{out}. The friction loss coefficient is calculated using the Manning formula

$$\zeta_f = \frac{2gLn^2}{R^{4/3}} \tag{5.9}$$

where L is the culvert length, n is Manning's coefficient and R is the mean hydraulic radius along the culvert. The Manning's n-value depends on the interior surface of the culvert. Table values can be found in literature. For example, a concrete culvert n would typically range from 0.011 to 0.017.

The bend loss coefficient, ζ_b, is provided for situations where head losses other than from the above occur, for example bends, damaged culverts, trapped debris. For straight culverts in good condition a value of zero would apply. The critical flows (and orifice flows for culverts as well) are multiplied by the critical flow correction factor, α_c, specified as the free overflow head loss factor. Typically, a value of 1.0 is used.

5.3 Composite structures

A composite structure is a combination of a number of weirs and short culverts (see Figure 5.8). A composite structure is defined as a cross section where total discharge across the cross section is calculated using empirical formulas for weirs and culverts and distributed along the cross section. In the numerical calculations the cross section is defined as a section of element faces which is treated as an internal discharge boundary (weak formulation). However, the flux contribution to the continuity equation is corrected to secure mass conservation. The approach for calculating the mean water level and for distribution of the total discharge are the same as the approach used for weirs and culverts.

The total discharge across the combined structures is calculated by iteration until a stable flow is achieved. During the iteration, the energy headloss of the structures is modified; thus, only structures that apply an energy description are modified in the iteration process. These include culverts and broad Crested Weirs. If none of these structures are present in a composite structure, then no iterations are performed.

A set of structures forming a composite structure are recognized from the location definitions. Locations must be completely identical for all the structures forming the composite structure. That is, the table of coordinates defining the structure locations must be exactly identical (number of coordinates and coordinate values) for all structures defined.

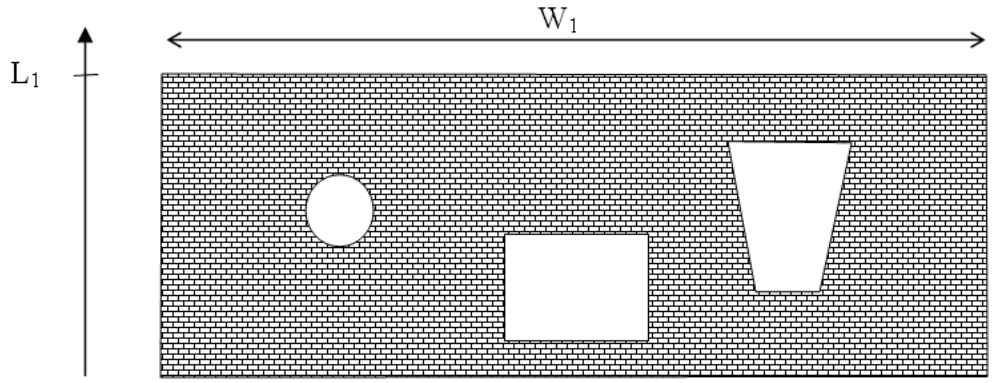

Figure 5.8 Setup definitions of a composite structure. Here the structure consists of one weir with a constant crest level L_1 and three short culverts (a circular, a rectangular and a irregular).

5.4 Dikes

A dike is defined as a cross section and in the numerical calculations the cross section is defined as a section of element faces which is treated as an internal discharge boundary (weak formulation). However, the flux contribution to the continuity equation is corrected to secure mass conservation. The discharge across each face in the section is calculated using an empirical formula or specified as input.

When the empirical formulation is used the discharge, q, over an element face with the length (width), Δl, is calculated based on the water level in the elements to the left and right of the face. The upstream water level is then the highest of the two water levels and the downstream water level the smallest. A standard weir expression, reduced according to the Villemonte formula, is applied

$$q = C(\eta_{US} - z_W)^k \left(1 - \frac{\eta_{DS} - z_W}{\eta_{US} - z_W}\right)^{-0.385} \Delta l \tag{5.10}$$

where C is the weir coefficient, k is the weir exponential coefficient, η_{US} is the upstream water level, η_{DS} is the downstream water level and z_W is the weir level taken with respect to the global datum (see Figure 5.9). The value of the weir exponent is 1.5 and the default value of the weir coefficient is 1.838.

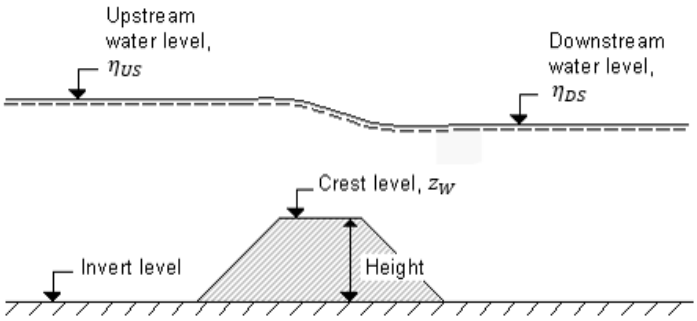

Figure 5.9 Definition sketch for dike flow.

5.5 Gates

A gate is defined as a cross section and in the numerical calculations the cross section is defined as a section of element faces. At an element face with the length, Δl, the normal flux is calculated as the sum of the normal flux for a solid wall, where the length is determined as $(1-c)\Delta l$, and the normal flux for a standard wet face, where the length is $c\Delta l$. Here, c is a weighting factor with a value between 0 and 1, where 0 corresponds to a closed gate and 1 corresponds to an open gate.

If the gate is defined for the full water column, c is equal to the user-defined gate control factor, c_{input}. If the gate geometry is defined as a subset of the water column the vertical location of the gate is defined by the top level, z_{top}, and bottom level of the gate, z_{bottom}, (see Figure 5.10). In this case *c* is calculated as

$$c = f c_{input} + (1 - f) \tag{5.11}$$

where f is the fraction of the water column, which is blocked by the gate. The surface elevation at the gate, η_{gate}, is obtained as the mean value of the surface elevation at elements to the left and to the right of the gate face and the bed level at the gate, z_{gate}, is obtained as the mean value of the bed level at elements to the left and to the right of the gate face.

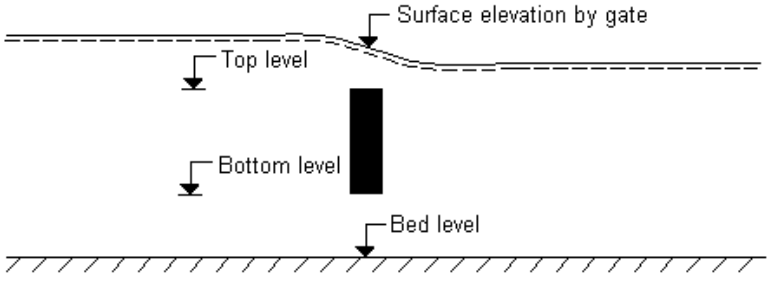

Figure 5.10 Definition sketch for gate flow.

5.6 Piers

The effect of piers is modelled as sub-grid structures by an additional volume force to the momentum equation in the column of cells where the pier is located. A simple drag-law is used to capture the increasing resistance imposed by the piers as the flow speed increases.

The effective current induced drag force, F_D, is determined from

$$F_D = \frac{1}{2}\rho_0 \gamma C_D A_e V^2 \tag{5.12}$$

where γ is the streamline factor, C_D is the drag coefficient, A_e is the effective area of the pier exposed to current and V is the current speed. The sign of F_D is such that a positive force acts against the current direction. The streamline factor is a factor that is multiplied on the total drag force to take into account the increased flow velocity due to the blocking of piers. The velocity is the velocity in the cell, where the pier is located

A pier is defined as a number of pier segments, which are vertical sections with different geometrical layout (see Figure 5.11 and Figure 5.12). The geometrical layout can be

- Circular
- Rectangular
- Elliptical

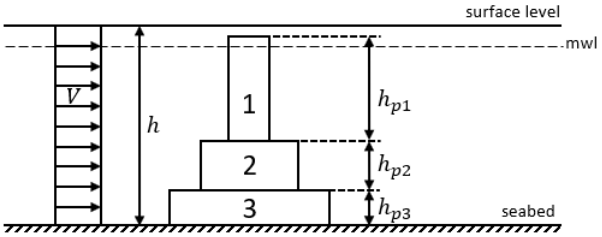

Figure 5.11 Pier with 3 sections with heights h_{p1}, h_{p2} and h_{p3}.

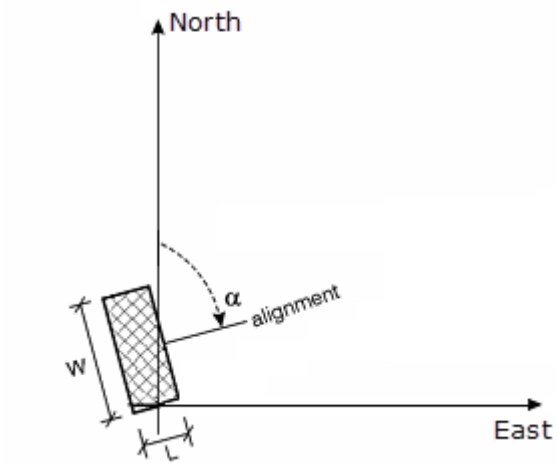

Figure 5.12 Definition of pier angles. w is the width of the pier section, L is the length of the pier section, α is the angle between projection north and the alignment.

5.7 Turbines

The effect of tidal turbines is modelled as sub-grid structures by an additional volume force to the momentum equation in the column of cells where the turbine is located. A simple drag-law is used to capture the increasing resistance imposed by the turbine blades as the flow speed increases. Turbines are assumed always to have their axis aligned with the flow direction.

The effect to the flow due to the turbines is modeled by calculating the current induced drag and lift force on each individual layer (see Figure 5.13). The effective drag force, F_D, and lift force, F_L, are determined from

$$F_D = \frac{1}{2}\rho_0 \alpha C_D A_e V^2 \tag{5.13}$$

$$F_L = \frac{1}{2}\rho_0 \alpha C_L A_e V^2 \tag{5.14}$$

where α is a correction factor, $C_D$is the drag coefficient, C_L is the lift coefficient, A_e is the effective area of the turbine exposed to current and V is the upstream current speed.

When no current correction is applied the upstream current velocity is approximated by the local velocity, V_{local}. The local velocity is the velocity in the cell, where the turbine is located. When current correction is included the upstream current speed is approximated by

$$V_0 = \frac{2}{1+\sqrt{1-\gamma}} V_{local} \tag{5.15}$$

where $\gamma = \alpha C_D A_e/(h\Delta s)$. Here h is the water depth and Δs is grid distance. When the drag coefficient is specified as a function of the upstream current speed the corrected current speed is determined by iteration. The grid distance is determined as the width perpendicular to the flow direction of the element, where the turbine is located. For more detail see (Kramer et al. (2014)).

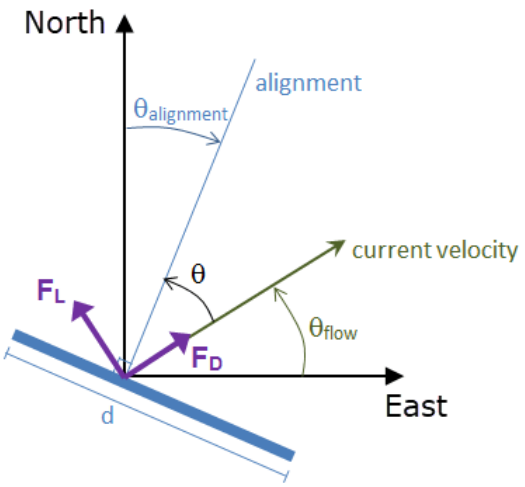

Figure 5.13 Definition of turbine angles. d is the diameter of the turbine, θ_{flow} is the current direction, $\theta_{alignment}$ is the angle between projection north and the alignment and θ is the angle between alignment and flow.

6 Parallelization

The MIKE 21 Flow Model FM utilizes the following parallelization techniques in a hybrid manner

- OpenMP computing approach
- MPI computing approach
- GPU computing approach

The MIKE 21 Flow Model FM is parallelized for shared-memory multiprocessor/multicore computers using OpenMP. This parallelization is performed by adding compiler directives to the code.

To improve performance and to be able to perform simulations on large massively parallel distributed-memory computers and clusters, MIKE 21 Flow Model FM has also been parallelized using the domain decomposition concept and Message Passing Interface (MPI). Given the number of processor cores allocated to a simulation, the computational mesh is partitioned into subdomains, and the workload associated with each domain is distributed between the allocated cores. The data exchange between domains is performed by message passing using the Intel MPI Library, which has multi fabric message passing capabilities. It allows the use of mixed communication between the domains. Thus, domains will exchange data via the fastest communication interface – in ranked order: shared memory, InfiniBand, Ethernet, etc..

The GPU computing approach uses the computers graphics card to perform the computational intensive calculations. This approach is based on CUDA™ by NVIDIA and can be executed on NVIDIA graphic cards with Compute Capability 3.0 or higher. Only the computational intensive part of the calculations solving the flow equations and transport equations (temperature and salinity and transport of a scalar quantity) are performed on the GPU. The additional calculations (e.g. input and output handling) are for each sub-domain performed on the CPU and these calculations are parallelized based on the OpenMP computing approach.

6.1 The domain decomposition

The domain partitioning is performed using the METIS graph partitioning library (Karypis and Kumar, (1998, 1999)). The computational mesh is converted into a graph, and then METIS uses a multi-level graph partitioning scheme to split the graph into subgraphs, representing the partitioned subdomains, which are distributed among the allocated cores. METIS computes a balanced partitioning that minimizes the connectivity of the subdomains and the difference in the number of elements in all subdomains.

The chosen numerical scheme for the discretization in the spatial domain requires an overlapping domain decomposition. It is based on the halo-layer (“ghost”-cells) approach, where each subdomain contains elements from connected subdomains. This overlap is needed, because calculations require values from the connecting elements. Thus, calculations of some elements at the border between subdomains require values from the connected subdomains.

6.2 Data exchange

The data exchange between processes is based on the aforementioned halo-layer (“ghost”-cells) approach with overlapping elements. The extension of the halo-layer area

depends on the numerical scheme used for the discretization in the spatial domain and which variables are chosen to be exchanged between subdomains. Here a two-element wide halo-layer is applied. The data exchanges are performed via asynchronous communication when possible, and synchronous communications are used in different parts of the system to ensure correct execution. The MIKE 21 Flow Model FM uses a dynamic time step in the time integration scheme. To ensure that the calculations are performed with the same time step in all subdomains, time step information is exchanged between processes and thereby synchronizing the processes of each time step. Several special features require additional data exchange. These special interest points cause synchronization of two or more subdomains during the data exchange. The case of input and output data exchange is mentioned in the next subsection. Finally, information is exchanged between subdomains in connection with error handling. When the system encounters an error in the model, the error is distributed to the other processes when the time step is finished and the simulation is stopped.

6.3 Input and output

The input and output (I/O) is handled using a parallel I/O approach. The master process reads the global mesh information, performs the partitioning of the mesh and distributes the information about the individual subdomains to the slave processes. Each process then reads the additional input specifications using the generic specification file. The input data (wind maps, initial condition maps, etc.) are read by each process using the global data files. Since the individual processes perform I/O locally, the simulation data files must be accessible by each process. This access could be through a network-attached storage system or locally on each computer. The output data files from the simulations are written to private files for each subdomain. At the end of the simulation, the data files are merged to obtain data files containing global information.

7 References

/1/ Aupoix, B. (1984), *Eddy Viscosity Subgrid Scale Models for Homogeneous Turbulence*, in Macroscopic Modelling of Turbulent Flow, Lecture Notes in Physics, Proc. Sophie-Antipolis, France.

/2/ Barth, T. J., and Jespersen, D. C. (1989), *The Design and Application of Upwind Schemes on Unstructured Meshes*, AIAA, paper 89-0366, Jan. 1989

/3/ Chan, D. T. L., Kennedy, J. F., and Lin, J. T. (1976), *Entrainment and drag forces of deflected jets.* Journal of the Hydraulics Division, 102(5), pp.615-635.

/4/ Chen, G., and Noelle, S. (2017), *A new hydrostatic reconstruction scheme based on subcell reconstructions*. SIAM Journal on Numerical Analysis, 55(2), 758-784.

/5/ Chippada, S., Dawson, C. N., Martinez, M. L., and Wheeler, M. F. (1998), *A Godunov-type finite volume method for the system of Shallow Water Equations*, Computational Methods in Applied Mechanics and Engineering, 151, 105-129.

/6/ Darwish, M. S., and Moukalled, F. (2003), *TVD schemes for unstructured grids*, Int. J. of Heat and Mass Transfer, 46, 599-611.

/7/ DHI, 2019, MIKE 3 Flow Model FM, Hydrodynamic and transport module, Scientific documentation.

/8/ Engelund, F. (1953), *On the laminar and turbulent flows of ground water through homogeneous sand*, Technical Report, Danish Academy of Technical Sciences.

/9/ Flather, R. A. (1976), *A tidal model of the northwest European continental shelf*, Memories de la Societe Royale des Sciences de Liege 6 (10), 141-164.

/10/ Fraccarollo, I., and Toro E. F. (1994), *Experimental and numerical assessment of the shallow water model for two-dimensional dam-break type problems*, Journal of Hydraulic Research 33, 951-979.

/11/ Fredsøe, J. (1984), *Turbulent boundary layers in Combined Wave Current Motion*, J. Hydraulic Engineering, ASCE, Vol 110, No. HY8, pp. 1103-1120.

/12/ Geernaert, G. L., and Plant, W. L (1990), *Surface Waves and fluxes, Volume 1 – Current theory*, Kluwer Academic Publishers, The Netherlands.

/13/ Harten, A., Lax, P. D., and Van Leer, B. (1983), *On upstream differencing and Godunov-type schemes for hyperbolic conservation-laws*, SIAM Rev 25(1), 54-74.

/14/ Hirsch, C. (1990), *Numerical Computation of Internal and External Flows,* Volume 2: Computational Methods for Inviscid and Viscous Flows, Wiley.

/15/ Holmes, D. G., and Connell, S. D. (1989), *Solution of the 2D Navier-Stokes on unstructured adaptive grids*, AIAA Pap. 89-1932 in Proc. AIAA 9th CFD Conference.

/16/ Horiuti, K. (1987), *Comparison of Conservative and Rotational Forms in Large Eddy Simulation of Turbulent Channel Flow*, Journal of Computational Physics, 71, pp 343-370.

/17/ Iqbal, M. (1983), *An Introduction to solar Radiation*, Academic Press.

/18/ Jawahar, P., and Kamath, H. (2000), *A high-resolution procedure for Euler and Navier-Stokes computations on unstructured grids*, Journal of Computational Physics, 164, 165-203.

/19/ Jones, O., Zyserman, J.A., and Wu, Y. (2014), *Influence of Apparent Roughness on Pipeline Design Conditions under Combined Waves and Current*, Proceedings of the ASME 2014 33rd International Conference on Ocean, Offshore and Arctic Engineering.

/20/ Kantha, L. H., and Clayson, C. A. (2000), *Small Scale Processes in Geophysical Fluid flows*, International Geophysics Series, Volume 67.

/21/ Karypis, G., and Kumar, V. (1998), *METIS: family of multilevel partitioning algorithms*, Available from: http://glaros.dtc.umn.edu/gkhome/views/metis.

/22/ Karypis, G., and Kumar, V. (1999), *A Fast and Highly Quality Multilevel Scheme for Partitioning Irregular Graphs*, SIAM Journal on Scientific Computing, Vol. 20, No. 1, 1999, pp. 359—392.

/23/ Kramer, S. C., Piggott, M. D., Hill, J., Kregting, L., Pritchard, D., and Elsaesser, B. (2014), *The modelling of tidal turbine farms using multi-scale, unstructured mesh models*, Proceedings of the 2nd International Conference on Environmental Interactions of Marine Renewable Energy Technologies (EIMR2014), 28 April - 02 May 2014, Stornoway, Isle of Lewis, Outer Hebrides, Scotland.

/24/ Lambert, J. D. (1973), *Computational Methods in Ordinary Differential Equations*, John Willey & Sons.

/25/ Leonard, A. (1974), *Energy Cascades in Large-Eddy Simulations of Turbulent Fluid Flows*, Advances in Geophysics, 18, pp 237-247.

/26/ Liang, Q., and Borthwick, A. G. L. (2009), *Adaptive quadtree simulation of shallow flows with wet-dry fronts over complex topography*, Computers and Fluids 38, 221-234.

/27/ Lilly, D. K. (1966), *On the Application of the Eddy Viscosity Concept in the Inertial Subrange of Turbulence*, NCAR Manuscript No. 123, National Center for Atmospheric Research, Boulder, Colorado.

/28/ Lindh, G., and Falkenmark, M. (1972), *Hydrology: en inledning till vattenressursläran*, tudentlitteratur (in Swedish).

/29/ Luhar, M., and Nepf, H. M. (2011), *Flow-induced reconfiguration of buoyant and flexible aquatic vegetation*, Limnol Oceanogr 56(6), 2003–17.

/30/ Luhar, M., and Nepf, H. M. (2013), *From the blade scale to the reach scale: A characterization of aquatic vegetative drag*, Advances in Water Resources 51, 305–316.

/31/ Naef, D., Rickenmann, D., Rutschmann, P., and McArdell, B. W. (2006), *Comparison of flow resistance relations for debris flows using a one-dimensional finite element simulation model*, Natural Hazards and Earth System Science, 6(1), 155-165.

/32/ Oddo, P., and Pinardi, N. (2007), *Lateral open boundary conditions for nested limited area models: A scale selective approach*, Ocean Modelling 20 (2008) 134-156.

/33/ Pugh, D. T. (1987), *Tides, surges and mean sea-level: a handbook for engineers and scientists*, Wiley, Chichester, 472pp.

/34/ Quecedo, M., and Pastor, M. (2002), *A reappraisal of Taylor-Galerkin algorithm for drying-wetting areas in shallow water computations*, International Journal for Numerical Methods in Fluids, 38, 515-531.

/35/ Rogers, B., Fujihara, M., and Borthwick, A. G. L. (2001), *Adaptive Q-tree Godunov-type scheme for shallow water equations*, International Journal for Numerical Methods in Fluids, 35, 247-280.

/36/ Sahlberg, J. (1984), *A hydrodynamic model for heat contents calculations on lakes at the ice formation date*, Document D4: 1984, Swedish council for Building Research.

/37/ Shu, C. W. (1997), *Essentially Non-Oscillatory and Weighted Essentially Non-Oscillatory Schemes for Hyperbolic Conservation Laws*, NASA/CR-97-206253, ICASE Report No. 97-65, NASA Langley Research Center, pp. 83.

/38/ Sleigh, P. A., Gaskell, P. H., Bersins, M., and Wright, N. G. (1998), *An unstructured finite-volume algorithm for predicting flow in rivers and estuaries*, Computers & Fluids, Vol. 27, No. 4, 479-508.

/39/ Smagorinsky, J. (1963), *General Circulation Experiment with the Primitive Equations*, Monthly Weather Review, 91, No. 3, 99-164.

/40/ Song, L., Zhou, J., Guo, J., Zou, Q., and Liu, Y. (2011), *A robust well-balanced finite volume model for shallow water flows with wetting and drying over irregular terrain*, Advances in Water Resources, vol. 34, no. 7, 915–932.

/41/ Stone, B. M., and Shen, H. T. (2002), *Hydraulic resistance of flow in channels with cylindrical roughness*, Journal of Hydraulic Engineering, 128(5), 500-506.

/42/ Toro, E. F. (2001), *Shock-capturing methods for free-surface flows*, Chichester, John Wiley & Sons.

/43/ Toro, E. F., Spruce, M., and Speares, W. (1994), *Restoration of the contact surface in the HLL-Riemann solver*, Shock Waves 4, 25–34.

/44/ UNESCO (1981), *The practical salinity scale 1978 and the international equation of state of seawater 1980*, UNESCO technical papers in marine science, 36, 1981.

/45/ van Gent, M. R. A. (1995), *Wave Interaction with Permeable Coastal Structures*, Ph.D. thesis, Delft University.

/46/ Vreugdenhill, C. B. (1994), *Numerical methods for shallow-water flow*, Water Science and Technology Library, Volume 13, Kluwer Academic Publishers.

/47/ Wolfram, P. J., and Fringer, O. B. (2013), *Mitigating horizontal divergence "checker-board" oscillations on unstructured triangular C-grids for nonlinear hydrostatic and nonhydrostatic flows*, Ocean Modelling, 69, 64-78.

/48/ Wu, J. (1994), *The sea surface is aerodynamically rough even under light winds*, Boundary layer Meteorology, 69, 149-158.

/49/ Wu, J. (1980), *Wind-stress Coefficients over sea surface and near neutral conditions – A revisit*, Journal of Physical. Oceanography, 10, 727-740.

/50/ Zhang, S., Zhao, X., and Bayyuk, S. (2014), *Generalized formulations for the Rhie-Chow interpolation*, Journal of computational Physics, 258, 880-914.

/51/ Zhao, D. H., Shen, H. W., Tabios, G. Q., Tan, W. Y., and Lai, J. S. (1994), *Finite volume 2-dimensional unsteady-flow model for river basins*, Journal of Hydraulic Engineering, ASCE, 1994, 120, No. 7, 863-833.

MIKE
Powered by DHI

APPENDICES

APPENDIX A – Governing equations in spherical coordinates

A Governing equations in spherical coordinates

In spherical coordinates the independent variables in the horizontal domain are the longitude, λ , and the latitude, ϕ. The horizontal velocity field (u,v) is defined by

$$u = Rcos\phi\frac{d\lambda}{dt} \qquad v = R\frac{d\phi}{dt} \tag{A. 1}$$

where R is the radius of the earth.

A.1 Governing equations in spherical coordinate system

A.1.1 Flow equations

The shallow water equations are given as

$$\frac{\partial h}{\partial t} + \frac{1}{Rcos\phi}\left(\frac{\partial hu}{\partial \lambda} + \frac{\partial hvcos\phi}{\partial \phi}\right) = 0 \tag{A. 2}$$

$$\frac{\partial hu}{\partial t} + \frac{1}{Rcos\phi}\left(\frac{\partial hu^2}{\partial \lambda} + \frac{\partial hvucos\phi}{\partial \phi}\right) =$$

$$\left(f + \frac{u}{R}tan\phi\right)hv - \frac{1}{Rcos\phi}\left(gh\frac{\partial \eta}{\partial \lambda} + \frac{h}{\rho_0}\frac{\partial p_A}{\partial \lambda} + \frac{gh^2}{2\rho_0}\frac{\partial \rho}{\partial \lambda}\right) - \frac{\tau_{fx}}{\rho_0} + \frac{\tau_{sx}}{\rho_0} \tag{A. 3}$$

$$+ \frac{1}{Rcos\phi}\frac{\partial hT_{xx}}{\partial \lambda} + \frac{1}{Rcos\phi}\frac{\partial hT_{xy}cos\phi}{\partial \phi}$$

$$\frac{\partial hv}{\partial t} + \frac{1}{Rcos\phi}\left(\frac{\partial huv}{\partial \lambda} + \frac{\partial hv^2cos\phi}{\partial \phi}\right) =$$

$$-\left(f + \frac{u}{R}tan\phi\right)hu - \frac{1}{R}\left(gh\frac{\partial \eta}{\partial \phi} + \frac{h}{\rho_0}\frac{\partial p_A}{\partial \phi} + \frac{h}{\rho_0}\frac{\partial p_A}{\partial \phi}\right) + hF_v - \frac{\tau_{fy}}{\rho_0} + \frac{\tau_{sy}}{\rho_0} \tag{A. 4}$$

$$+ \frac{1}{Rcos\phi}\frac{\partial hT_{xy}}{\partial \lambda} + \frac{1}{Rcos\phi}\frac{\partial hT_{yy}cos\phi}{\partial \phi}$$

$$T_{xx} = 2\nu\frac{1}{Rcos\phi}\frac{\partial u}{\partial \lambda} \quad T_{xy} = \nu\frac{1}{Rcos\phi}\left(\frac{\partial u}{\partial \lambda} + \frac{\partial vcos\phi}{\partial \phi}\right) \quad T_{yy} = 2\nu\frac{1}{Rcos\phi}\frac{\partial ucos\phi}{\partial \phi} \tag{A. 5}$$

A.1.2 Transport equations

The transport equation for, temperature and salinity are given as

$$\frac{\partial hT}{\partial t} + \frac{1}{Rcos\phi}\left(\frac{\partial huT}{\partial \lambda} + \frac{\partial hvTcos\phi}{\partial \phi}\right) = \frac{1}{R^2cos^2\phi}\frac{\partial}{\partial \lambda}\left(hD_{ts}\frac{\partial T}{\partial \lambda}\right) + \frac{1}{R^2cos\phi}\frac{\partial}{\partial \phi}\left(hD_{ts}\frac{\partial Tcos\phi}{\partial \phi}\right) + h\widehat{H} \tag{A. 6}$$

$$\frac{\partial hS}{\partial t} + \frac{1}{Rcos\phi}\left(\frac{\partial huS}{\partial \lambda} + \frac{\partial hvScos\phi}{\partial \phi}\right) = \frac{1}{R^2 cos^2\phi}\frac{\partial}{\partial \lambda}\left(hD_{ts}\frac{\partial S}{\partial \lambda}\right) + \frac{1}{R^2 cos\phi}\frac{\partial}{\partial \phi}\left(hD_{ts}\frac{\partial Scos\phi}{\partial \phi}\right) \quad \text{(A. 7)}$$

The transport equation for a scalar quantity is given as

$$\frac{\partial hC}{\partial t} + \frac{1}{Rcos\phi}\left(\frac{\partial huC}{\partial \lambda} + \frac{\partial hvCcos\phi}{\partial \phi}\right) = \frac{1}{R^2 cos^2\phi}\frac{\partial}{\partial \lambda}\left(hD_c\frac{\partial C}{\partial \lambda}\right) + \frac{1}{R^2 cos\phi}\frac{\partial}{\partial \phi}\left(hD_c\frac{\partial Ccos\phi}{\partial \phi}\right) - hk_pC \quad \text{(A. 8)}$$

MIKE
Powered by DHI

APPENDIX B – Governing equations for porous media

B Governing equations for porous media

The porosity $n = n(x, y)$ is defined as the fraction of a volume that is filled with fluid. Consider a given volume V, where the fluid fills the volume V_p and the rest is filled with solid material. Then the porosity is defined as

$$n = \frac{V_p}{V} \tag{B. 1}$$

Let $\boldsymbol{u} = (u, v)$ be the velocity inside the fluid. Then the superficial volume average, or the filter velocity, is defined as

$$\langle \boldsymbol{u} \rangle = \frac{1}{V} \int_{V_p} \boldsymbol{u} \, dV \tag{B. 2}$$

The intrinsic volume average, or the pore velocity, is defined as

$$\langle \boldsymbol{u} \rangle^f = \frac{1}{V_p} \int_{V_p} \boldsymbol{u} \, dV \tag{B. 3}$$

These volume averages are related by $\langle \boldsymbol{u} \rangle = n \langle \boldsymbol{u} \rangle^f$. In the following, the velocities, and other variables, refer to intrinsic volume averages unless explicitly stated otherwise.

B.1 Governing equations for porous media

B.1.1 Flow equations

The shallow water equations are given as

$$\frac{\partial nh}{\partial t} + \frac{\partial nhu}{\partial x} + \frac{\partial nhv}{\partial y} = 0 \tag{B. 4}$$

$$\begin{aligned}(1 + c_m)\frac{\partial nhu}{\partial t} + \frac{\partial nhu^2}{\partial x} + \frac{\partial nhuv}{\partial y} = \\ fnhv - gnh\frac{\partial \eta}{\partial x} - \frac{nh}{\rho_0}\frac{\partial p_A}{\partial x} - \frac{gnh^2}{2\rho_0}\frac{\partial \rho}{\partial x} - n\frac{\tau_{fx}}{\rho_0} + n\frac{\tau_{sx}}{\rho_0} - nF_{vx} - nF_{px} \\ + \frac{\partial hT_{xx}}{\partial x} + \frac{\partial hT_{xy}}{\partial y}\end{aligned} \tag{B. 5}$$

$$\begin{aligned}(1 + c_m)\frac{\partial nhv}{\partial t} + \frac{\partial nhvu}{\partial x} + \frac{\partial nhv^2}{\partial y} = \\ -fnhu - gnh\frac{\partial \eta}{\partial y} - \frac{nh}{\rho_0}\frac{\partial p_A}{\partial y} - \frac{gnh^2}{2\rho_0}\frac{\partial \rho}{\partial y} - n\frac{\tau_{fy}}{\rho_0} + n\frac{\tau_{sy}}{\rho_0} - nF_{vy} - nF_{py} \\ + \frac{\partial hT_{xy}}{\partial x} + \frac{\partial hT_{yy}}{\partial y}\end{aligned} \tag{B. 6}$$

$$T_{xx} = 2\nu\frac{\partial nu}{\partial x} \qquad T_{xy} = \nu\left(\frac{\partial nu}{\partial y} + \frac{\partial nv}{\partial x}\right) \qquad T_{yy} = 2\nu\frac{\partial nu}{\partial y} \tag{B. 7}$$

$\boldsymbol{F}_p = (F_{px}, F_{py})$ is the friction force due to porosity.

B.1.2 Transport equations

The transport equations for the intrinsic volume averages of temperature and salinity are given as

$$\frac{\partial nhT}{\partial t}+\frac{\partial nhuT}{\partial x}+\frac{\partial nhvT}{\partial y}=\frac{\partial}{\partial x}\left(nhD_{ts}\frac{\partial T}{\partial x}\right)+\frac{\partial}{\partial y}\left(nhD_{ts}\frac{\partial T}{\partial y}\right)+nh\widehat{H} \tag{B. 8}$$

$$\frac{\partial nhS}{\partial t}+\frac{\partial nhuS}{\partial x}+\frac{\partial nhvS}{\partial y}=\frac{\partial}{\partial x}\left(nhD_{ts}\frac{\partial S}{\partial x}\right)+\frac{\partial}{\partial y}\left(nhD_{ts}\frac{\partial S}{\partial y}\right) \tag{B. 9}$$

The transport equation for the intrinsic volume average of a scalar quantity is given as

$$\frac{\partial nhC}{\partial t}+\frac{\partial nhuC}{\partial x}+\frac{\partial nhvC}{\partial y}=\frac{\partial}{\partial x}\left(nhD_{c}\frac{\partial C}{\partial x}\right)+\frac{\partial}{\partial y}\left(nhD_{c}\frac{\partial C}{\partial y}\right)-nhk_{p}C \tag{B. 10}$$